

**WIDE BAND ELECTRO-OPTIC INTENSITY MODULATOR
FREQUENCY RESPONSE MEASUREMENT USING OPTICAL HETERODYNE,
DOWN-CONVERSION TECHNIQUE**

by

ALFRED KAN MIN LAM

B. A. Sc., The University of British Columbia, 2002

A THESIS SUBMITTED IN PARTIAL FULFILMENT OF
THE REQUIREMENTS FOR THE DEGREE OF
MASTER OF APPLIED SCIENCE

in

THE FACULTY OF GRADUATE STUDIES

(Electrical and Computer Engineering)

THE UNIVERSITY OF BRITISH COLUMBIA

March 2005

© Alfred Kan Min Lam, 2005

Abstract

In this thesis a novel system for measuring the frequency responses of electro-optic intensity modulators in the millimeter-wave regime is described. As the frequency responses of modulators increase, wide band, and cost effective methods to measure these responses need to be developed. The system described in this thesis uses optical heterodyning and a wide band photodiode to generate millimeter-waves to drive the device under test (DUT). The need for a wide band microwave sweeper can therefore be eliminated. Moreover, an inexpensive frequency shifter consisting of a Mach-Zehnder modulator and an optical bandpass filter is used to down-convert the output of the DUT to a low microwave frequency at which the output is easily measured. The system measures $|S_{21}|$ in dBe.

The system can measure the frequency responses of different types of electro-optic intensity modulators such as Mach-Zehnder modulators, mode-converter modulators, electro-optic polymer modulators, and should also work for electroabsorption modulators. In this thesis, the frequency response measurement system is described, and mathematical expressions for the optical fields at the output of an electro-optic modulator are developed when the DUT is biased or operated at its maximum, quadrature, and minimum points. High frequency measurements on a 10 Gb/s LiNbO₃ Mach-Zehnder type modulator and a 40 Gb/s GaAs mode-converter type modulator are made. The measurements show close agreement with $|S_{21}|$ measurements made using vector network analyzers and calibrated wide band photodiodes.

In addition, the harmonic rejection feature of our system is described. Our system “rejects” higher order harmonics, due to the non-linearities, generated in the DUT with proper selection of the modulation and the shift frequencies. This feature means that our system can measure the linear frequency response of the DUT even if it is operated, or biased, in a non-linear region.

Table of Contents

Abstract.....	ii
List of Figures.....	v
List of Tables.....	viii
Acknowledgements.....	ix
Co-authorship.....	x
Chapter 1. Introduction.....	1
1.1. Literature Review and Motivation.....	1
1.2. Thesis Overview.....	4
1.3. Supplementary Information on the Settings of the Measurement System.....	5
References.....	7
Chapter 2. Electro-optic Intensity Modulator Frequency Response Measurement.....	9
2.1. Introduction.....	9
2.2. Optical Heterodyne, Down-conversion Technique Theory.....	11
2.2.1. Modulator Optical Signal.....	11
2.2.2. Frequency Response Measurement System.....	16
2.3. Experimental Results.....	23
2.3.1. Wide Band Measurements.....	23
2.3.2. Harmonic Rejection.....	31
2.4. Conclusion.....	33
References.....	34
Chapter 3. Summary, Conclusions and Recommendations for Future Work.....	37
3.1. Summary and Discussions.....	37
3.2. Recommendations for Future Work.....	40
References.....	42
Appendices.....	43
Appendix A. Optical Heterodyning.....	43
Appendix B. The Frequency Shifter.....	46
Appendix C. Harmonic Rejection Requirements.....	52
Appendix D. Electro-optic Intensity Modulator Frequency Response Measurement using Vector Network Analyzer.....	55
Appendix E. Comparison of the System Dynamic Range of our System to that of a VNA.....	59
References.....	63

List of Figures

- Figure 2.1. Schematic diagram showing the measurement system used.
PC: Polarization Controller, ATTN: Optical Attenuator,
WPD: Wide Band Photodiode, LPD: Low Frequency Photodiode,
BPT: Optical Bandpass Filter, MZI: Mach-Zenhder 17
- Figure 2.2. Uncorrected frequency responses of the 10 Gb/s modulator
measured using our system from 1 to 65 GHz and the VNA
from 45 MHz to 50 GHz. The residual power signal of our system
is shown as the dashed line..... 25
- Figure 2.3. Corrected frequency responses of the 10 Gb/s modulator
measured using our system from 1 to 50 GHz and the VNA
from 45 MHz to 50 GHz..... 26
- Figure 2.4. Three measurements showing the corrected frequency responses
of the 10 Gb/s modulator using our system up to 60 GHz.
The repeatability was +/- ~1 dB.....27
- Figure 2.5. Uncorrected frequency responses of the 40 Gb/s modulator
measured using our system from 1 to 78 GHz and the VNA
from 40 MHz to 65 GHz. The residual power signal of our system
is shown as the dashed line..... 29
- Figure 2.6. Corrected frequency responses of the 40 Gb/s modulator
measured using our system from 1 GHz to 50 GHz and the VNA
from 40 MHz to 50 GHz.....30

Figure 2.7. Detected signals for f_m equals 10 GHz. The detected signals are at a) $f_s = 2.4$ GHz); b) $f_m - f_s$ (=7.6 GHz); c) f_m (=10 GHz); d) $f_m + f_s$ (=12.4 GHz); e) $2f_m - f_s$ (=17.6 GHz); f) $2f_m$ (=20 GHz).....	32
Figure A.1. A setup of an optical heterodyne system. PC: Polarization Controller, WPD: Wide band Photodiode.....	43
Figure B.1. Diagram showing the setup of the frequency shifter used in the measurement system.....	46
Figure B.2. The 3-dB pass-band of the filter was measured to be ~1558.47 nm to ~1558.66 nm.....	47
Figure B.3. Spectrum of the optical components from the frequency shifter and the DUT. a) The component from the frequency shifter, b) the high frequency sideband from the DUT, c) the low frequency sideband from the DUT, d) the optical carrier from the DUT. (Setting of the ANDO AQ6317B optical spectrum analyzer: RBW = 0.01 nm, Span = 1 nm).....	49
Figure B.4. Diagram showing the system used to obtain the optical field shown in Figure B.3.....	50
Figure D.1. The VNA setup used to measure the frequency response of the DUTs in Chapter 2. WPD: Wide Band photodiode.....	55
Figure E.1. Our system showing a higher system dynamic range than that of the 50 GHz VNA.....	60

Figure E.2. The frequency response of the modulator when no laser source was supplied is shown as the dotted curve. It overshadowed the uncorrected frequency response of the 10 Gb/s modulator measured using the VNA, shown as the solid curve, starting at ~45 GHz. The uncorrected frequency responses of the 10 Gb/s modulator measured using our system, shown as the asterisks, shows continual roll-off beyond 50 GHz due to the virtually flat power output from the optical heterodyning and the constant residual power signal shown as the dashed line. 62

List of Tables

Table 2.1. Optical and microwave frequencies as in Figure 2.1.....17

Table C.1. Table showing the frequencies of the electrical signals at the output of the low frequency photodiode due to the mixing of the signals at the output of the frequency shifter with the signals at the output of the DUT. 53

Acknowledgements

My deepest appreciation goes to my parents for their love, trust, and support throughout my life including the course of this work. I would like to extend my sincere gratitude to my supervisor, Dr. N.A. F. Jaeger, for proposing this project and providing continual support during my research. His dedication and friendly guidance has been most invaluable to me in the course of this program.

I would like to thank Sasa Ristic for his consistent encouragement during the course of this work, and his helpful comments and discussions regarding my research. I would also like to thank all the individuals in the electro-optics lab, department office, part ordering, and ... all others who have helped me. Finally, I would like to thank my family and friends for their encouragement, especially my girlfriend, Joyce Chang, for her love and understanding.

Co-authorship

Alfred Kan Min Lam conducted research, designed the measurement system, performed experiments, collected measurement data and analysed the data, and provided the first draft of the manuscript.

Mair Fairburn measured the frequency response of the 40 Gb/s mode converter modulator using a 65 GHz VNA (Anritsu 37397C) shown in Figures 2.5 and 2.6. He also provided professional input and guidance regarding high speed measurement and feedback regarding the manuscript.

Nicolas A.F. Jaeger provided input regarding the design of the measurement system and helped write the manuscript.

Chapter 1

Introduction

1.1 Literature Review and Motivation

Recent advances in optoelectronic technology have resulted fiber optic communications networks and systems with bandwidth in the tens-of-gigahertz. The realization of wide bandwidth systems has been achieved by the development of wide band optoelectronic devices, such as photodiodes or photoreceivers and electro-optic modulators. For instance, the bandwidths of commercially available photodiodes currently exceed 50 GHz [1-3] and of electro-optic intensity modulators exceed 40 GHz [4-6]. At present, electro-optic intensity modulators with bandwidths in the 100 GHz range are under development [7-9]. The interest in ultrawide band electro-optic modulators is due to the simplicity of AM photodetection in intensity modulation and is currently the most popular scheme, as compared to phase, frequency, and polarization modulation [10].

Most commonly, the frequency responses of electro-optic intensity modulators are measured using a vector network analyzer (VNA) with a calibrated photodiode, or a lightwave component analyzer, see for example [11-14]. These analyzers provide a means to easily measure the modulator's characteristics such as its amplitude and phase response. These analyzers are costly, especially for frequencies of 50 GHz and above.

Therefore, wide band, cost effective methods need to be developed to measure the frequency responses of these modulators.

Besides the analyzers described above, several techniques that are used to measure the frequency responses of electro-optic intensity modulators can be found in the literature, but the measurements are limited to frequencies of 50 GHz and below [15-17]. In 1978, Shingo Uehara proposed a swept frequency technique to measure the frequency response of an electro-optic intensity modulator from 0.1 to 2 GHz. In the technique, an amplitude modulated RF sweeper was used to drive the device under test (DUT), and a crystal (square law) detector and a lock-in amplifier were used to measure the responses [15].

In 1989, Tan et al. reported an optical modulator frequency response measurement using a Nd:YAG ring laser heterodyne technique [16]. In the technique, the DUT was stimulated with a small RF modulation signal and was supplied an optical source from a laser. A second laser was mixed with the DUT to down-convert the sideband of the DUT to a constant RF frequency using a photodiode. The power of the signal at the constant RF frequency was then easily measured using an electrical spectrum analyzer. The frequency range of the system was limited by the bandwidth of the microwave sweeper used.

Another electro-optic intensity modulator frequency response measurement system was suggested by Watson et al. in 1993 [17]. In the system, a Mach-Zehnder modulator biased at its minimum transmission point was used as both a mixer and a frequency doubler. The output of this modulator was used as an optical input to the DUT that was operated at its linear region and was driven by an RF signal from a microwave

sweeper. The response of the modulator was then measured in a lightwave component analyzer. Again, the frequency range of the suggested system was limited by the bandwidth of the microwave sweeper used.

The system described in this thesis does not need a costly wide bandwidth microwave sweeper; instead, it uses optical heterodyning and a wide band photodiode to generate a millimeter-wave to drive a DUT. Moreover, the system has the potential to increase its frequency range by using a wider band photodiode to meet the continuing increase in the bandwidth of electro-optic intensity modulators.

1.2 Thesis Overview

Chapter 2 is a manuscript that has been submitted to the “IEEE Transactions on Microwave Theory and Techniques”. In the manuscript, a novel system for measuring the frequency responses of electro-optic intensity modulators at millimeter-wave frequencies is presented. High frequency measurements on both a 10 Gb/s Mach-Zehnder type modulator and a 40 Gb/s mode converter type modulator are made. The optical fields at the output of an electro-optic modulator when it is biased, or operated, at three different points on its transfer function are derived. In addition, the harmonic rejection feature of the system is described, which “rejects” higher order harmonics generated by non-linearities in the DUT.

Chapter 3 gives a summary of the work conducted, conclusions and suggestions for improving the performance of the measurement system and for reducing the cost of the system.

Chapter 4 contains five appendices. Appendix A describes the generation of millimeter-wave using optical heterodyning. Appendix B describes the design of the frequency shifter used in the measurement system. Appendix C describes how the system “rejects” the higher order harmonics and the requirements of achieving the rejection property. Appendix D shows how a VNA and a calibrated wide band photodiode are used to measure the frequency response of an electro-optic intensity modulator. Appendix E compares the system dynamic range of the measurement system to that of the Agilent 8150C VNA used.

1.3 Supplementary Information on the Settings of the Measurement System

The power of laser 1 (Agilent 81682A, with option 3^{*}) was set at 6.5 dBm, which was its maximum setting for the wavelength range covered in the experiments to measure the two DUTs, starting at 1558.4280 nm. The power of laser 2 (Agilent 81682A, without option 3) was maximized to 8.273 dBm, at 1558.4200 nm. The microwave power of a 1 GHz signal generated at the output of the 55 GHz photodiode (manufactured by Discovery Semiconductor Inc.) was estimated to be ~ -8 dBm using an electrical spectrum analyzer.

The two DUTs and the Mach-Zehnder modulator in the frequency shifter were both operated, or biased, at their minimum points to maximize the sensitivity of the system, as will be described in Chapter 2. The Mach-Zehnder modulator in the frequency shifter was a 10 Gb/s LiNbO₃ modulator (serial #: 277-171L) manufactured by JDS Uniphase Ltd. Its DC input voltage was set at ~ 2.6 Volts in order to bias it at the minimum point. The power and frequency of the signal that stimulated the modulator in the frequency shifter were 18 dBm and 2.4 GHz, respectively. The DC input voltages to the two DUTs were ~ 2.6 Volts (the 10 Gb/s modulator) and ~ 12 Volts (the 40 Gb/s modulator), respectively.

The low frequency photodiode used was manufactured by Discovery Semiconductor Inc. (model number: DSC-30H). The two DUTs were a 10 Gb/s Mach-Zehnder modulator (serial #: 325-662H) manufactured by JDS Uniphase Ltd. and a 40

^{*} Option 3 is a 60 dB built-in variable attenuator that reduces the maximum power by ~ 1.5 dB.

Gb/s mode converter modulator (serial #:0059-R03) manufactured by JGKB Photonics Inc.

The two wide band photodiodes used in the measurement system are as follows:

1. PIN diode (DSC 10H)¹; Manufacturer: Discovery Semiconductor Inc.
2. Waveguide-integrated photodetector (XPDV2020R)²; Manufacturer: U²T Photonics Inc.

The span, resolution bandwidth, and the video bandwidth of the electrical spectrum analyzer (Agilent E4407B) were set at 500 kHz, 10 kHz and 100 Hz, respectively, when the response data were taken.

¹ This photodiode was used in the system to measure the $|S_{21}|$ of the 10 Gb/s modulator.

² This photodiode was used in the system to measure the $|S_{21}|$ of the 40 Gb/s modulator.

References

- [1] T. S. Clement, D. F. Williams, P. D. Hale, and J. M. Morgan, "Calibrating photoreceiver response to 110 GHz," *National Institute of Standards and Technology*.
- [2] "DC to 65 GHz wide bandwidth InGaAs photodiodes and photoreceivers," Application Note, DISCOVERY SEMICONDUCTORS, New Jersey, March 2000.
- [3] "50 GHz High Responsivity" Preliminary Data Sheet, U²T PHOTONICS, Berlin, Germany.
- [4] N. Dagli, "Wide-bandwidth lasers and modulators for RF photonics," *IEEE Tran. On Microwave Theory and Techniques*, vol. 47, No. 7, pp. 1151-1171, July 1999.
- [5] F. Rahmatian, N. A. F. Jaeger, R. James, and E. Berolo, "An ultrahigh-speed AlGaAs-GaAs polarization converter using slow-wave coplanar electrodes," *IEEE Photon. Technol. Lett.*, vol. 10, pp. 675-677, 1998.
- [6] M. M. Howerton, R. P. Moeller, A. S. Greenblatt, and R. Krahenbuhl, "Fully packaged, broad-band LiNbO₃ modulator with low drive voltage," *IEEE Photon., Technol. Lett.*, vol. 12, pp. 792-794, Jul. 2000.
- [7] K. Noguchi, O. Mitomi, and H. Miyazawa, "Millimeter-wave Ti:LiNbO₃ optical modulators," *J. of Lightwave Technology*, vol. 16, No. 4, pp. 615-619, 1998.
- [8] D. Chen, H. Fetterman, A. Chen, W. H. Steier, L. R. Dalton, W. Wang, and Y. Shi, "Demonstration of 110 GHz electrooptic polymer modulators," *Appl. Phys. Lett.*, vol. 70, no. 25, pp. 3335-3337, 1997.
- [9] K. W. Hui, B. Y. Wu, Y. M. Choi, J. H. Peng, and K. S. Chiang, "Design of modified phase reversal electrode in broad-band electrooptic modulators at 100 GHz," *IEEE Tran. On Microwave Theory and Techniques*, vol. 45, No. 1, pp. 142-145, Jan. 1997.

- [10] G. L. Li, and P. K. L. Yu, "Optical intensity modulators for digital and analog applications," *J. of Lightwave Technology*, vol. 21, No. 9, pp. 2010-2030, Sep. 2003.
- [11] "MN4765A O/E Calibration module," Operation Manual, Anritsu, Morgan Hill, CA.
- [12] M. Matsumoto, "Fast electro-optical phase modulators completely measured in frequency and time domains," *Electronics letters*, vol. 25, No. 23, pp. 1569-1571, Nov. 1989.
- [13] "Agilent 8703B Lightwave Component Analyzer," Technical Specifications, Agilent Technologies, Palo Alto, CA.
- [14] "Agilent 86030A Lightwave Component Analyzer," Product Overview, Agilent Technologies, Palo Alto, CA.
- [15] S. Uehara, "Calibration of optical modulator frequency response with application to signal level control," *Appl. Opt.*, vol. 17, pp. 68-71, 1978.
- [16] Tun S. Tan, Roger L. Jungerman, and Scott S. Elliott, "Optical receiver and modulator frequency response measurement with a Nd:YAG ring laser heterodyne technique," *IEEE Tran. On Microwave Theory and Techniques*, vol. 37, No. 8, pp. 1217-1222, 1989.
- [17] C. D. Watson, D. A. Humphreys, and M. G. F. Wilson, "Calibration of optical modulators by optical down-conversion," *IEEE Photonics Technology Letters*, vol. 5, No. 9, pp. 1005-1007, Sep. 1993.

Chapter 2*

Electro-optic Intensity Modulator Frequency Response Measurement

2.1. Introduction

Ultrahigh speed electro-optic intensity modulators play an important role in wide band fiber optic communication systems. Modulators operating at speeds of 40 Gb/s are currently commercially available and modulators operating at speeds in the 100 GHz range are under development. These include modulators made in LiNbO_3 [1]-[4], III-V compound semiconductors [5]-[8], and electro-optic polymers [9]-[11].

As the frequency responses of optical modulators increase, cost effective methods by which to measure these responses need to be developed. Here we present a technique to measure the electro-optic $|S_{21}|$ that uses optical heterodyning and a wide band photodiode to make measurements at millimeter-wave frequencies.

Optical heterodyning is used in the calibration of photodiodes and optical receivers as it offers the most accurate method for measuring their frequency responses [12]-[14]. In this method, a tunable laser is mixed with another laser at the photodiode to generate a beat frequency in the microwave regime.

In our system, we heterodyne two lasers at a wide band photodiode to generate a millimeter-wave that drives the device under test (DUT). Clearly, two lasers that can be tuned to have a wavelength difference of ~ 1 nm have a difference frequency of ~ 125

* A version of this chapter has been submitted to "IEEE Transactions on Microwave Theory and Techniques" for publication.

GHz at 1550 nm. Therefore, optical heterodyning can provide a cost effective method to do measurements at ultrahigh frequencies by eliminating the need for an ultrawide band microwave sweeper.

2.2. Optical Heterodyne, Down-conversion Technique Theory

Our system can measure the frequency responses of different types of electro-optic intensity modulators such as Mach-Zehnder modulators, mode-converter modulators, electro-optic polymer modulators, and should be able to measure the frequency response of electroabsorption modulators. In what follows, we will develop mathematical expressions for the optical fields at the output of a Mach-Zehnder type modulator when it is biased or operated at its maximum, quadrature, and minimum points in a small-signal modulation analysis. Next, the system used to measure the frequency response of a DUT is presented, followed by a discussion of the harmonic rejection feature of our system.

2.2.1. Modulator Optical Signal

Here we assume a balanced electro-optic intensity modulator with the following transfer function, i.e., with zero intrinsic bias [15]

$$I_{out}(V) = I_o \cos^2\left(\frac{\pi V}{2V_\pi}\right) \quad (1)$$

where I_o is the maximum output intensity, V_π is the half-wave voltage of the modulator, and V is the applied voltage given by

$$V = V_{DC} + V_{RF} \quad (2)$$

or

$$V = V_{DC} + V_m \cos(2\pi f_m t). \quad (3)$$

where V_{DC} is a DC voltage, V_{RF} is an RF voltage, V_m and f_m are the amplitude and the frequency of the RF, or microwave, signal.

Substituting equation (3) into (1), we find that the optical field at the output of the modulator can be written as

$$E_{out} = 2\sqrt{\frac{\mu_o}{\epsilon}} I_{out}^{1/2} (V) = 2\sqrt{\frac{\mu_o}{\epsilon}} I_o^{1/2} \cos(\phi_{DC} + \phi_{RF}) \cdot e^{j2\pi f t} \quad (4)$$

where μ_o is the permeability of free space, ϵ is the permittivity of the material,

$$\phi_{DC} = \frac{\pi V_{DC}}{2V_\pi} \text{ and } \phi_{RF} = \frac{\pi V_m}{2V_\pi} \cos(2\pi f_m t) \text{ or } \phi_{RF} = M \cos(2\pi f_m t), \text{ i.e., } M = \frac{\pi V_m}{2V_\pi}, \text{ and } f \text{ is}$$

the frequency of the light. The term $\cos(\phi_{DC} + \phi_{RF})$ can be expressed using Taylor expansion and Bessel functions about the microwave frequency, f_m , see for example [16]-[18],

$$\begin{aligned} \cos(\phi_{DC} + \phi_{RF}) = & \cos \phi_{DC} \left\{ J_0(M) + 2 \sum_{n=1}^{+\infty} (-1)^n J_{2n}(M) \cos[2n(2\pi f_m t)] \right\} \\ & - \sin \phi_{DC} \left\{ -2 \sum_{n=1}^{+\infty} (-1)^n J_{2n-1}(M) \cos[(2n-1)(2\pi f_m t)] \right\} \end{aligned} \quad (5)$$

where J_n is the Bessel function of the first kind of order n .

For small-signal modulation (i.e., $M \ll 1$), we have

$$J_0(M) \approx 1, \quad (6a)$$

$$J_1(M) \approx M/2, \quad (6b)$$

$$J_{2n}(M) \approx 0 \text{ for } 1 \leq n < +\infty, \quad (6c)$$

and

$$J_{2n-1}(M) \approx 0 \text{ for } 2 \leq n < +\infty. \quad (6d)$$

When the modulator is operated at its maximum point (i.e., $\phi_{DC} = 0$, $\cos \phi_{DC} = 1$, and $\sin \phi_{DC} = 0$), then equations (5) and (4) can be approximated, respectively, as

$$\cos(\phi_{DC} + \phi_{RF}) = 1 \quad (7)$$

and

$$E_{out} = 2\sqrt{\frac{\mu_o}{\varepsilon}} I_o^{1/2} e^{j2\pi ft} = 2\sqrt{\frac{\mu_o}{\varepsilon}} I_o^{1/2} \cos(2\pi ft) \quad (8)$$

The optical signal at the output of the modulator consists of only one optical component at the frequency of the light source, f , and no first order sidebands are present.

When the modulator is operated at its quadrature point (i.e., $\phi_{DC} = \pi/4$, and $\cos \phi_{DC} = \sin \phi_{DC} = 1/\sqrt{2}$), then equations (5) and (4) can be approximated, respectively, as

$$\cos(\phi_{DC} + \phi_{RF}) = \frac{1}{\sqrt{2}} [1 - M \cos(2\pi f_m t)] \quad (9)$$

and

$$\begin{aligned} E_{out} &= \sqrt{\frac{2\mu_o}{\epsilon}} I_o^{1/2} [1 - M \cos(2\pi f_m t)] e^{j2\pi f t} \\ &= \sqrt{\frac{2\mu_o}{\epsilon}} I_o^{1/2} \cos(2\pi f t) - \sqrt{\frac{\mu_o}{2\epsilon}} I_o^{1/2} M \{ \cos[2\pi(f + f_m)t] + \cos[2\pi(f - f_m)t] \} \quad (10) \end{aligned}$$

As can be seen in equation (10), the signal has an optical carrier at frequency f and two sidebands, one at $f - f_m$ and the other one at $f + f_m$. As ϕ_{DC} increases towards $\pi/2$, the amplitude of the optical carrier, $\cos \phi_{DC} \cdot J_0(M)$, decreases while the amplitudes of the first sidebands, $\sin \phi_{DC} \cdot J_1(M)$, increase. The amplitude increase in the first sidebands enhances the sensitivity of our system, and the amplitude increases in other sidebands do not affect our measurement as they are “rejected”, as will be explained below.

When the modulator is operated at its minimum point (i.e., $\phi_{DC} = \pi/2$, $\cos \phi_{DC} = 0$, $\sin \phi_{DC} = 1$), then equations (5) and (4) can be approximated, respectively, as

$$\cos(\phi_{DC} + \phi_{RF}) = -M \cos(2\pi f_m t) \quad (11)$$

and

$$\begin{aligned}
 E_{out} &= -2\sqrt{\frac{\mu_o}{\varepsilon}} I_o^{1/2} M \cos(2\pi f_m t) e^{j2\pi f t} \\
 &= -\sqrt{\frac{\mu_o}{\varepsilon}} I_o^{1/2} M \{ \cos[2\pi(f + f_m)t] + \cos[2\pi(f - f_m)t] \} \quad (12)
 \end{aligned}$$

As shown in equation (12), the optical carrier is completely suppressed and the first sidebands are at the optical frequencies, $f - f_m$ and $f + f_m$. Actually, the extinction ratio of a particular modulator will place a limit on the amount to which the carrier can be suppressed. Nevertheless, the amplitudes of the first sidebands are the largest when the modulator is operated at this point.

As can be seen in equations (8), (10), and (12), the amplitudes of the first sidebands are maximum and minimum when the DUT is operated at its minimum and maximum points, respectively. Their amplitudes increase as the operating point is changed from the maximum point to the minimum point in the transfer function. The increase in the amplitudes of the first sidebands enhances the sensitivity of our system as it measures the frequency response by shifting one of the first sidebands to a constant frequency in a low frequency photodiode and rejects higher order harmonics due to the non-linearities generated in the modulator. Thus, for an electro-optic intensity modulator with a transfer function such as that given in equation (1), our system gives the best or highest sensitivity when it is operated at its minimum point. Nevertheless, our system can easily measure electro-optic intensity modulators that are biased in their linear regime, with a small penalty as regards the sensitivity, for example, 3 dB at the quadrature point.

2.2.2. Frequency Response Measurement System

A schematic diagram of the system used to measure the frequency response of the modulator (DUT) is shown in Figure 2.1. Table 2.1 shows the optical and microwave frequencies present when the DUT is biased at any point other than its maximum point. The optical signals are labeled 1 to 5 and the microwave signals are labeled A to C, where the mixing of higher order harmonics is neglected. (Note: In an improved, dedicated system, all of the EDFAs and three of the polarization controllers could be eliminated.)

Our system uses the outputs of the two lasers to generate a millimeter-wave signal to drive the DUT at the difference frequency

$$f_m = f_2 - f_1 \quad (13)$$

where f_1 and f_2 are the frequencies of lasers 1 and 2, respectively. Appendix A shows the details how a millimeter-wave signal can be generated by optical heterodyning. We also use a portion of the output of laser 1 as the optical input to the DUT, so that the output of the DUT has optical frequency components $f_1, f_1 + f_m$, and $f_1 - f_m$. Furthermore, we take a portion of the output from laser 2 as the optical input to the frequency shifter and shift its frequency by f_s (the shift frequency) from f_2 to $f_2 - f_s$. When we combine this shifted optical signal with the signals at the output of the DUT using a 50/50-coupler, we obtain optical components at $f_2 - f_s, f_1, f_1 + f_m$, and $f_1 - f_m$. These optical signals are then mixed using a low frequency photodiode giving

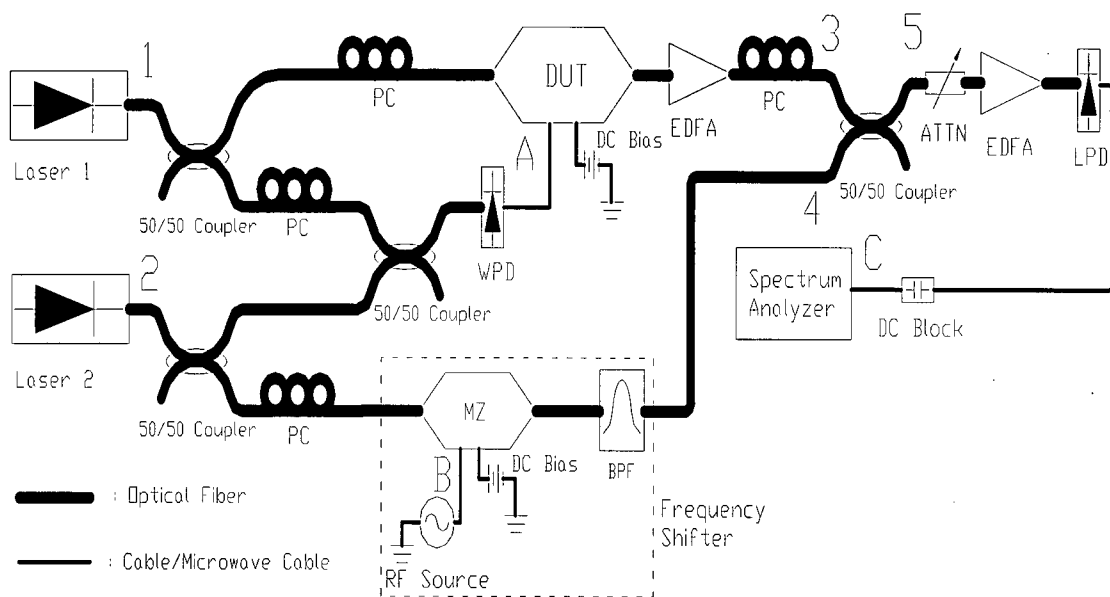


Figure 2.1. Schematic diagram showing the measurement system used. PC: Polarization Controller, ATTN: Optical Attenuator, WPD: Wide Band Photodiode, LPD: Low Frequency Photodiode, BPF: Optical Bandpass Filter, MZ: Mach-Zehnder

TABLE I
 OPTICAL AND MICROWAVE FREQUENCIES AS IN FIG. 1

The optical frequencies in the fibers	The microwave frequencies in the cables
1: f_1	A: f_m
2: f_2	B: f_s
3: $f_1 - f_m, f_1, f_1 + f_m$	C: $f_s, f_m - f_s, f_m, 2f_m - f_s, 2f_m$
4: $f_2 - f_s$	
5: $f_2 - f_s, f_1 - f_m, f_1, f_1 + f_m$	

down-converted components at $f_s, f_m - f_s, f_m, 2f_m - f_s,$ and $2f_m$. In particular, the high frequency sideband of the DUT at $f_1 + f_m$ mixes with the constant optical field from the frequency shifter at $f_2 - f_s$ to give an electrical signal at $(f_1 + f_m) - (f_2 - f_s)$, or rearranging, at $(f_1 - f_2 + f_m) + f_s$, or since $(f_2 - f_1) = f_m$, at f_s . Therefore, we use the term at the shift frequency, f_s , to measure the frequency response of the DUT.

In the following, we show how the frequency response can be measured at the shift frequency. The photocurrent resulting from heterodyning the signals from the tunable lasers, when properly mixed at the wide band photodiode is given as

$$i_{wpd} = R_{wpd} [P_{1m} + P_{2m} + 2 \cdot \rho_{wpd} \cdot \sqrt{P_{1m} P_{2m}} \cdot \cos(2\pi f_m t)] \quad (14)$$

where P_{1m} and P_{2m} are the optical powers from the two lasers that reach the wide band photodiode, R_{wpd} is the DC responsivity and ρ_{wpd} is the frequency response of the wide band photodiode. The DC term in equation (14) is constant and can be compensated for by adjusting the DC bias voltage. For small-signal modulation and neglecting the second and higher sidebands, the optical field at the output of the DUT, which is due to the heterodyne signal at f_m can be written as

$$E_{DUT} \propto E_{oDUT} [\cos \phi_{DC} J_0(M) - \sin \phi_{DC} J_1(M) \cdot \cos(2\pi f_m t)] e^{j2\pi f_1 t} \quad (15)$$

and the optical field at the output of the frequency shifter can be written as

$$E_{fs} \propto E_{ofs} e^{j2\pi(f_2-f_s)t} \quad (16)$$

where E_{oDUT} and E_{ofs} are the amplitudes of the optical fields at the outputs of the DUT and the frequency shifter, respectively. Appendix B provides information on the design of the frequency shifter used.

The following is a mathematical description of the mixing of the optical fields in the low frequency photodiode. When the optical fields in equations (15) and (16) are mixed in the low frequency photodiode, the detected photocurrent is given as

$$i_{lpd} = R_{lpd} \rho_{lpd} (E_{DUT} + E_{fs}) \cdot (E_{DUT}^* + E_{fs}^*) \quad (17)$$

where R_{lpd} and ρ_{lpd} are the DC responsivity and the frequency response of the low frequency photodiode, respectively. Expanding equation (17) (and squaring i_{lpd}), the electrical power at the various frequencies is

$$P_{elec} \propto \left(\frac{i_{lpd}}{R_{lpd} \rho_{lpd}} \right)^2 = P_{DC} + P_{f_s} + P_{f_m-f_s} + P_{f_m} + P_{2f_m-f_s} + P_{2f_m} \quad (18)$$

where

$$P_{DC} \propto [E_{ofs}^2 + E_{oDUT}^2 J_0^2(M) \cos^2 \phi_{DC} + \frac{1}{2} E_{oDUT}^2 J_1^2(M) \sin^2 \phi_{DC}]^2 \quad (19a)$$

$$P_{f_s} \propto E_{oDUT}^2 E_{ofs}^2 J_1^2(M) \sin^2 \phi_{DC} \cos(2\pi f_s t)$$

$$\approx \frac{1}{4} E_{oDUT}^2 E_{ofs}^2 M^2 \sin^2 \phi_{DC} \cos(2\pi f_s t) \quad (19b)$$

$$\begin{aligned} P_{f_m - f_s} &\propto E_{oDUT}^2 E_{ofs}^2 J_0^2(M) \cos^2 \phi_{DC} \cos[2\pi(f_m - f_s)t] \\ &\approx E_{oDUT}^2 E_{ofs}^2 \cos^2 \phi_{DC} \cos[2\pi(f_m - f_s)t] \end{aligned} \quad (19c)$$

$$\begin{aligned} P_{f_m} &\propto E_{oDUT}^4 J_0^2(M) J_1^2(M) \sin^2(2\phi_{DC}) \cos(2\pi f_m t) \\ &\approx \frac{1}{4} E_{oDUT}^4 M^2 \sin^2(2\phi_{DC}) \cos(2\pi f_m t) \end{aligned} \quad (19d)$$

$$P_{2f_m - f_s} = P_{f_s} \quad (19e)$$

$$\begin{aligned} P_{2f_m} &\propto E_{oDUT}^4 J_1^4(M) \sin^4 \phi_{DC} \cos(4\pi f_m t) \\ &\approx \frac{1}{16} E_{oDUT}^4 M^4 \sin^4 \phi_{DC} \cos(4\pi f_m t), \end{aligned} \quad (19f)$$

and the subscripts $f_s, f_m - f_s, f_m, 2f_m - f_s$, and $2f_m$ are the frequencies of the detected electrical signals $P_{f_s}, P_{f_m - f_s}, P_{f_m}, P_{2f_m - f_s}$ and P_{2f_m} , that are measured using the spectrum analyzer. The DC power, P_{DC} , can be filtered out by a DC block. The term at f_m is the AM signal. The terms at $f_m - f_s$ and $2f_m - f_s$ are the down-converted components due to the mixing of the output of the frequency shifter with the optical carrier at the output of the DUT and the mixing of the output of the frequency shifter with the lower frequency sideband at the output of the DUT, respectively. The term at $2f_m$ is due to the mixing of the two sidebands. The term at the shift frequency, f_s , is due to the mixing of the output of the frequency shifter with the higher frequency sideband of the DUT and is proportional to M^2 . M^2 gives the electrical frequency response of the DUT that we

want to measure, and $|S_{21}|$ is simply M^2 properly scaled. As shown in equation (19b), the power at f_s is maximized when ϕ_{DC} equals $\pi/2$. This implies that the highest sensitivity of our system can be obtained when the DUT is operated at the minimum point at which point the largest amplitude first sidebands are produced. M^2 can be obtained by normalizing the microwave power at f_s with respect to that of the calibrated electrical frequency response of the wide band photodiode. The normalized response gives us the frequency response, $|S_{21}|$, in dBe.

When the non-linear characteristics in the DUT are taken into account, the higher order harmonics are “rejected” by the optical field at the output of the frequency shifter. To show how these harmonics are “rejected”, the term $\cos(\phi_{DC} + \phi_{RF})$ in equation (5) is expanded and substituted into equation (4), and the optical field at the output of the DUT is

$$\begin{aligned}
 E_{DUT} \propto E_{oDUT} \{ & \cos \phi_{DC} [J_0(M) - 2J_2(M) \cos(4\pi f_m t) + 2J_4(M) \cos(8\pi f_m t) - \dots] \\
 & - \sin \phi_{DC} [2J_1(M) \cos(2\pi f_m t) - 2J_3(M) \cos(6\pi f_m t) \\
 & + 2J_5(M) \cos(10\pi f_m t) - \dots] \} e^{j2\pi f_s t}
 \end{aligned} \tag{20}$$

When the optical signals in equations (16) and (20) are mixed in the low frequency photodiode, the electrical powers generated are given as

$$\begin{aligned}
 P_{f_s} & \propto E_{oDUT}^2 E_{ofs}^2 J_1^2(M) \sin^2 \phi_{DC} \cos(2\pi f_s t) \\
 & \approx \frac{1}{4} E_{oDUT}^2 E_{ofs}^2 M^2 \sin^2 \phi_{DC} \cos(2\pi f_s t)
 \end{aligned} \tag{21a}$$

$$\begin{aligned}
P_{f_m-f_s} &\propto E_{oDUT}^2 E_{ofs}^2 J_0^2(M) \cos^2 \phi_{DC} \cos[2\pi(f_m - f_s)t] \\
&\approx E_{oDUT}^2 E_{ofs}^2 \cos^2 \phi_{DC} \cos[2\pi(f_m - f_s)t]
\end{aligned} \tag{21b}$$

$$P_{2f_m-f_s} = P_{f_s} \tag{21c}$$

$$\begin{aligned}
P_{if_m} &\propto E_{oDUT}^4 \sin^2(2\phi_{DC}) [J_0(M)J_i(M) + J_1(M)J_{i+1}(M) \\
&\quad + J_2(M)J_{i+2}(M) + J_3(M)J_{i+3}(M) + \dots]^2 \cdot \cos(2\pi if_m t)
\end{aligned} \tag{21d}$$

$$\begin{aligned}
P_{jf_m} &\propto E_{oDUT}^4 [\sin^2 \phi_{DC} J_{j/2}^2(M) + 2 \cos^2 \phi_{DC} \cdot J_0(M)J_j(M) + 2 \sin^2 \phi_{DC} J_1(M)J_{j+1}(M) \\
&\quad + 2 \cos^2 \phi_{DC} J_2(M)J_{j+2}(M) + 2 \sin^2 \phi_{DC} J_3(M)J_{j+3}(M) + \dots]^2 \cdot \cos(2\pi jf_m t)
\end{aligned} \tag{21e}$$

$$\begin{aligned}
P_{lf_m} &\propto E_{oDUT}^4 [\cos^2 \phi_{DC} J_{l/2}^2(M) + 2 \cos^2 \phi_{DC} J_0(M)J_l(M) \\
&\quad + 2 \sin^2 \phi_{DC} J_1(M)J_{l+1}(M) + 2 \cos^2 \phi_{DC} J_2(M)J_{l+2}(M) \\
&\quad + 2 \sin^2 \phi_{DC} J_3(M)J_{l+3}(M) + \dots]^2 \cdot \cos(2\pi lf_m t)
\end{aligned} \tag{21f}$$

$$P_{(k-1)f_m+f_s} \propto E_{oDUT}^2 E_{ofs}^2 J_k^2(M) \cdot \cos\{2\pi[(k-1)f_m + f_s]\} \tag{21g}$$

and

$$P_{(k+1)f_m-f_s} \propto E_{oDUT}^2 E_{ofs}^2 J_k^2(M) \cdot \cos\{2\pi[(k+1)f_m - f_s]\} \tag{21h}$$

where $i = 1, 3, 5, 7, \dots, j = 2, 6, 10, 14, \dots, l = 4, 8, 12, 16, \dots$ and $k = 2, 3, 4, 5, \dots$

The DC power is not shown here as it can be filtered out by a DC block. Again, the term at the shift frequency, f_s , in equation (21a) is the same as the term in equation (19b), where the higher order harmonics are neglected. Nevertheless, they are both proportional to the electrical frequency response of the DUT, M^2 . The terms in equations (21d), (21e) and (21f) are due to the mixing of the optical fields of the DUT itself. For example,

$$\begin{aligned}
P_{f_m} &\propto E_{oDUT}^4 J_0^2(M) J_1^2(M) \sin^2(2\phi_{DC}) \cos(2\pi f_m t) \\
&\approx \frac{1}{4} E_{oDUT}^4 M^2 \sin^2(2\phi_{DC}) \cos(2\pi f_m t)
\end{aligned} \tag{22}$$

and

$$\begin{aligned}
P_{2f_m} &\propto E_{oDUT}^4 [\sin^2 \phi_{DC} J_1^2(M) + 2 \cos^2 \phi_{DC} J_0(M) J_2(M)]^2 \cos(4\pi f_m t) \\
&\approx E_{oDUT}^4 [\sin^2 \phi_{DC} M^2 / 4 + 2 \cos^2 \phi_{DC} J_2(M)]^2 \cos(4\pi f_m t)
\end{aligned} \tag{23}$$

as $J_0(M)J_1(M)$ and $[\sin^2 \phi_{DC} J_1^2(M) + 2 \cos^2 \phi_{DC} J_0(M)J_2(M)]$ are the dominant coefficients in equations (21d) and (21e), respectively. The higher order harmonics generated in the DUT are shifted by the optical field at the output of the frequency shifter to frequencies of $(k-1)f_m + f_s$, and $(k+1)f_m - f_s$, as shown in equations (21g) and (21h). One can easily select f_m and f_s to ensure that none of the higher order harmonics is shifted to f_s . To do this, one must have $f_s \neq \frac{q}{r} f_m$, where q and r are any integers greater than zero. Appendix C shows how this requirement can be obtained in order to have none of the higher order harmonics shifted to f_s . This harmonic rejection means that our system can measure the linear frequency response of the DUT even if it is operated in a non-linear region.

2.3. Experimental Results

2.3.1. Wide Band Measurements

Frequency response measurements on both a 10 Gb/s LiNbO₃ Mach-Zehnder type modulator and a 40 Gb/s GaAs mode converter type modulator have been made. Laser 1 was swept from 1558.4280 nm and laser 2 was fixed at 1558.4200 nm, i.e., starting at a nominal 1 GHz difference. Both modulators were operated at their minimum points to obtain large amplitudes of the first sidebands. The shift frequency, f_s , was set at 2.4 GHz. The Mach-Zehnder modulator in the frequency shifter was operated at its minimum point to suppress the optical carrier and an optical bandpass filter was used to further suppress the carrier and to filter out the higher frequency sidebands. While not optimal, this frequency shifter was inexpensive to implement and was readily available. Nevertheless, an extremely small residual carrier remains. The response signals of the 10 Gb/s and the 40 Gb/s modulators at 1 GHz were about 32 dB and 37 dB above the residual power signal at f_s , respectively.

For comparison purposes, Figure 2.2 shows the “uncorrected” frequency response of the 10 Gb/s modulator measured using our system from 1 to 65 GHz as asterisks, the “uncorrected” frequency response of the modulator measured using an Agilent 8510C vector network analyzer (VNA) from 45 MHz to 50 GHz as the solid curve, and the residual power signal as the dashed line. By “uncorrected”, we mean that the measurement is not corrected by the frequency response of the wide band photodiode used. Appendix D shows how the frequency response of an electro-optic intensity modulator can be measured by a VNA. As can be seen, the two uncorrected responses

are in good agreement, but our system continues to give values above 50 GHz. Figure 2.3 shows the “corrected” frequency responses, M^2 and $|S_{21}|$, of the modulator up to 50 GHz. Figure 2.4 shows three measurements of the corrected frequency responses, M^2 , of the 10 Gb/s modulator up to 60 GHz (the maximum frequency for which this wide band photodiode was calibrated). The repeatability was $\pm \sim 1$ dB.

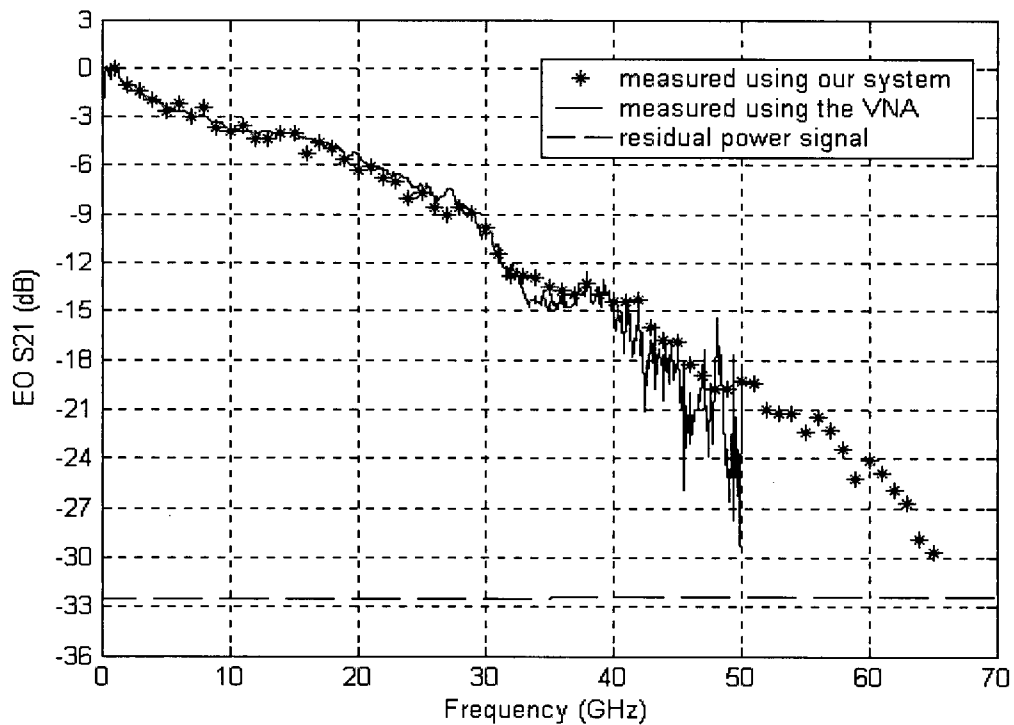


Fig. 2.2. Uncorrected frequency responses of the 10 Gb/s modulator measured using our system from 1 to 65 GHz and the VNA from 45 MHz to 50 GHz. The residual power signal of our system is shown as the dashed line.

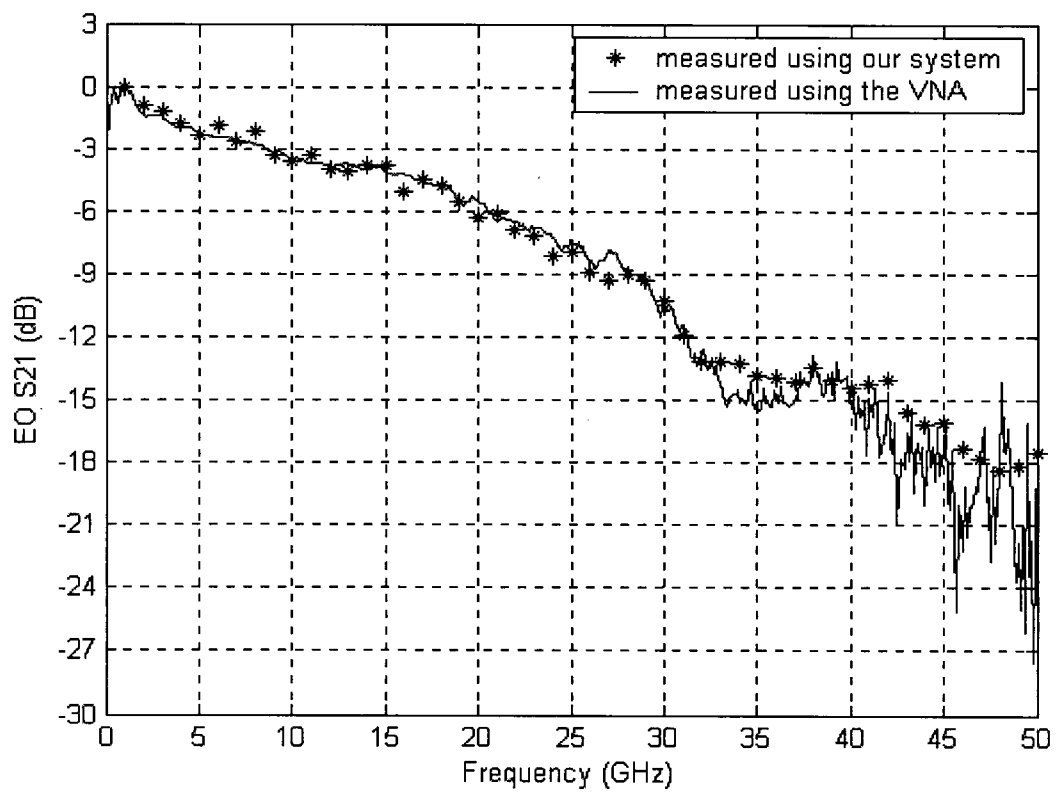


Fig. 2.3. Corrected frequency responses of the 10 Gb/s modulator measured using our system from 1 to 50 GHz and the VNA from 45 MHz to 50 GHz.

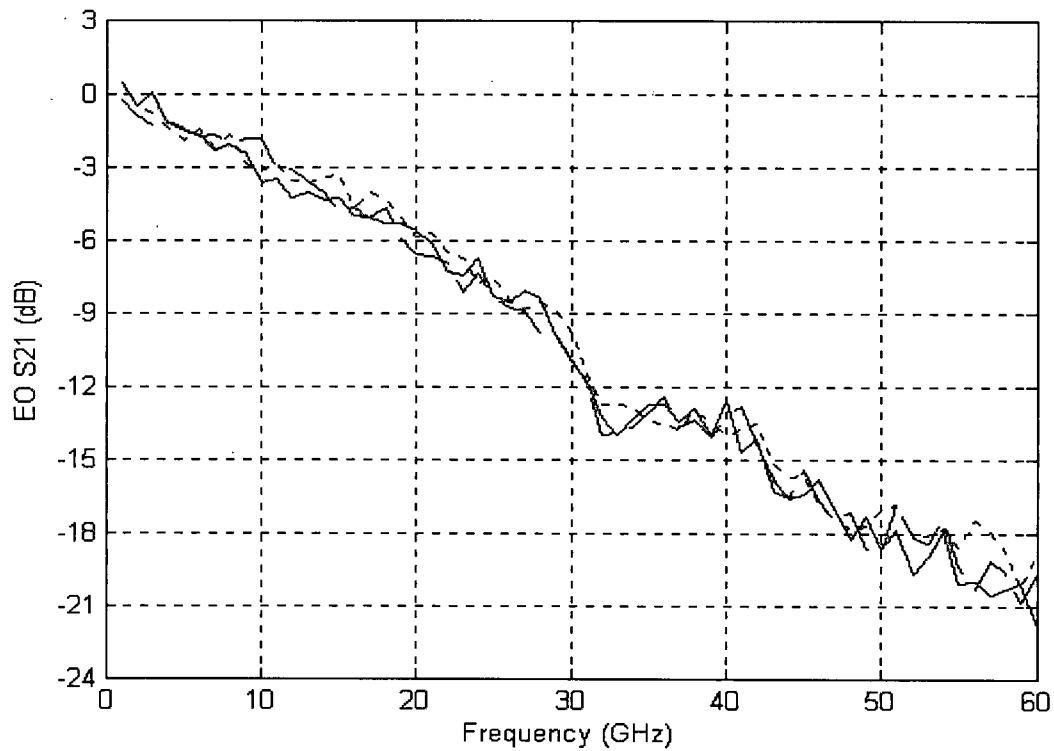


Fig. 2.4. Three measurements showing the corrected frequency responses of the 10 Gb/s modulator using our system up to 60 GHz. The repeatability was ± 1 dB.

Next, the frequency response of the 40 Gb/s modulator was measured using our system with a different wide band photodiode; this was the photodiode that was used by the modulator manufacturer to measure $|S_{21}|$ using a 65 GHz VNA (Anritsu 37397C). Figure 2.5 shows the uncorrected response of the 40 Gb/s modulator measured using our system from 1 GHz to 78 GHz as asterisks, the uncorrected frequency response measured using the 65 GHz VNA as the solid curve, and the residual power signal as the dashed line. Again, the two measurements are in good agreement. The response of the modulator measured using our system continues to roll off up to 78 GHz, at which frequency the response power was ~ 2 dB above the residual power signal. Figure 2.6 shows the corrected frequency responses, M^2 and $|S_{21}|$, of the modulator up to 50 GHz (the maximum frequency for which this wide band photodiode was calibrated). Both responses show the 3-dB electrical point at ~ 45 GHz.

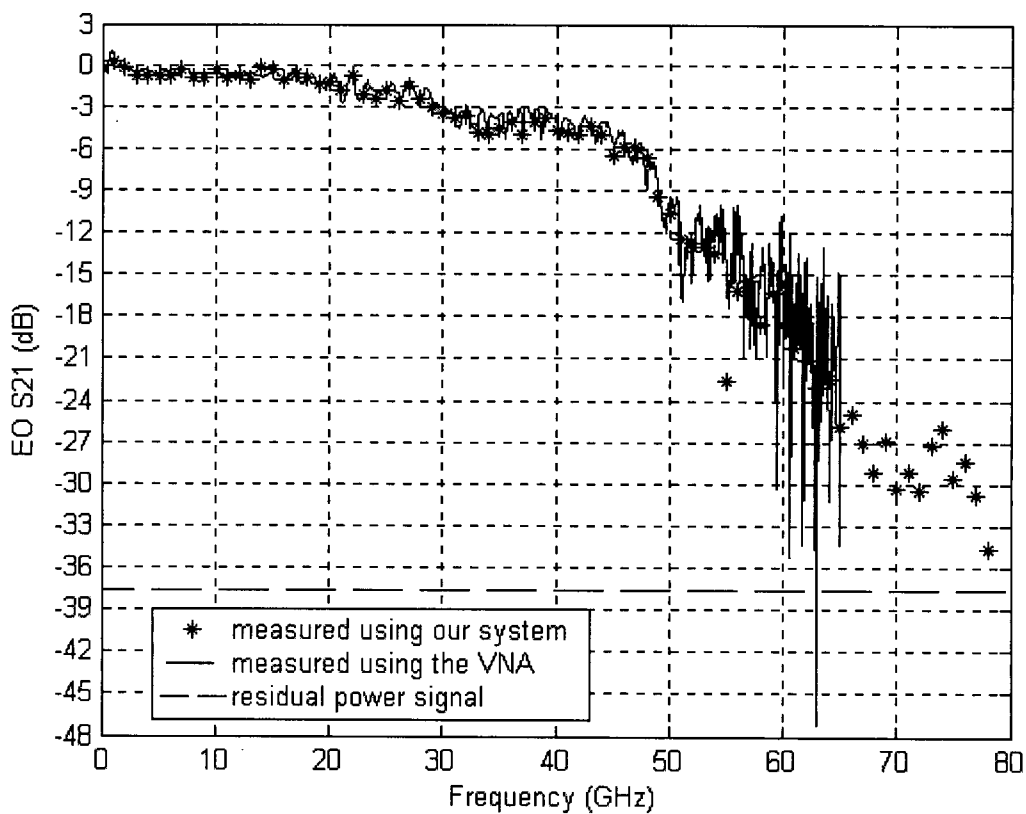


Figure 2.5. Uncorrected frequency responses of the 40 Gb/s modulator measured using our system from 1 to 78 GHz and the VNA from 40 MHz to 65 GHz. The residual power signal of our system is shown as the dashed line.

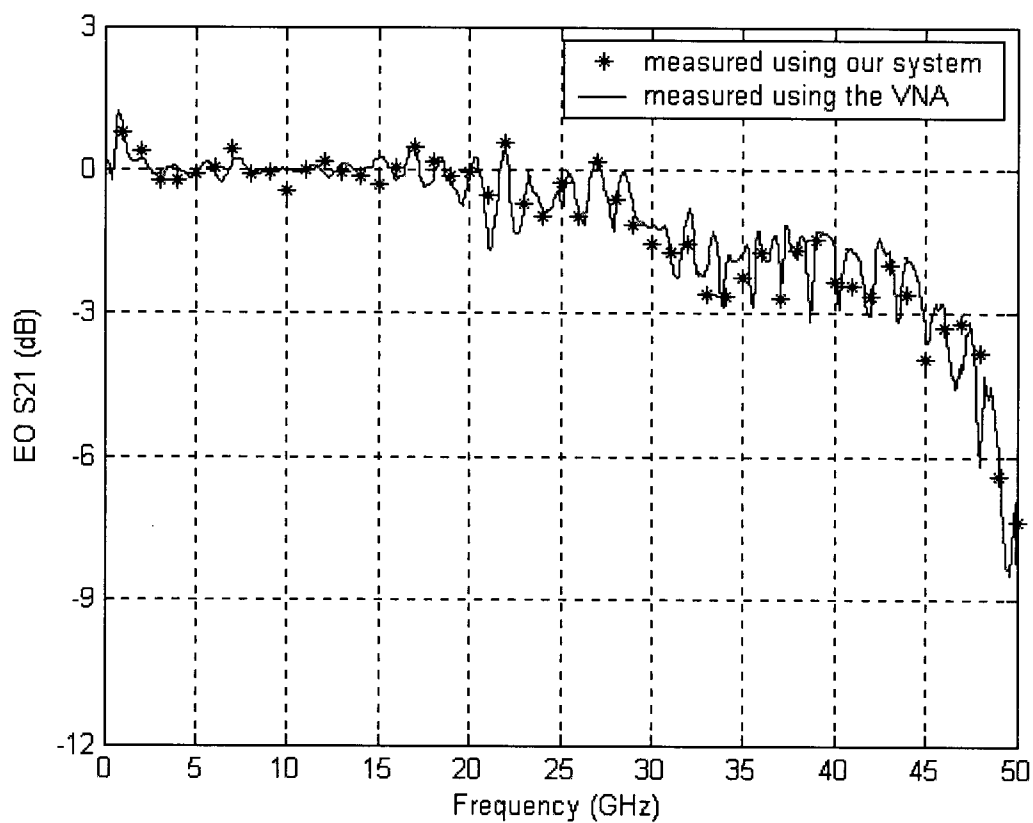


Figure 2.6. Corrected frequency responses of the 40 Gb/s modulator measured using our system from 1 GHz to 50 GHz and the VNA from 40 MHz to 50 GHz.

2.3.2. Harmonic Rejection

As discussed previously, one important feature of our system is that it rejects higher order harmonics generated in the DUT.

When the DUT is modulated by a signal with the difference frequency, f_m , the higher harmonics are shifted to frequencies of $(k-1)f_m + f_s$ and $(k+1)f_m - f_s$ where $k = 2, 3, 4, 5, \dots$ and is the order of the harmonic as shown in equations (21g) and (21h). As an example, Figure 2.7 shows the spectrum of the detected electrical signals using a 25 GHz photodiode as the “low frequency” photodiode, a wide band electrical spectrum analyzer and a DC block when f_m equals 10 GHz. The DUT is biased in its linear region to obtain higher amplitudes of the rejected signals. As can be seen, the signals labeled (a) and (e) are the frequency response of the DUT at frequencies f_s and $2f_m - f_s$ (see equations (21a) and (21c)). Signal (b), at $f_m - f_s$, is due to the mixing of the carrier at the output of the DUT and the optical field at the output of the frequency shifter, see equation (21b). (c) is the AM signal of the DUT at f_m , see equation (22). (d) is the shifted second harmonic signal at $f_m + f_s$ (see equation (21g) when $k = 2$), and signal (f), at $2f_m$, is mainly due to the mixing of the carrier and the second sidebands of the DUT and the mixing of the two first sidebands of the DUT (see equation (23)). Signal (f) is large as a result of a large second harmonic generated by the wide band photodiode used.

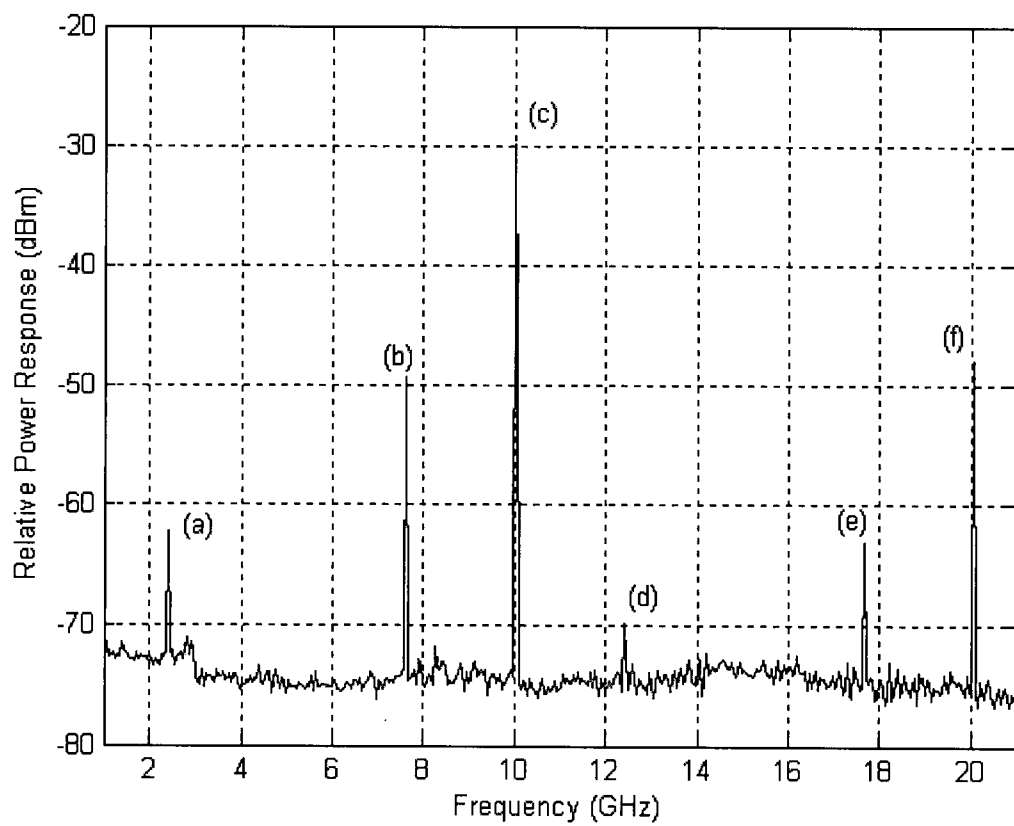


Figure 2.7. Detected signals for f_m equals 10 GHz. The detected signals are at a) f_s (=2.4 GHz); b) $f_m - f_s$ (=7.6 GHz); c) f_m (=10 GHz); d) $f_m + f_s$ (=12.4 GHz); e) $2f_m - f_s$ (=17.6 GHz); f) $2f_m$ (=20 GHz).

2.4 Conclusion

In this paper we have presented a novel system for measuring the frequency responses of electro-optic intensity modulators at millimeter-wave frequencies. High frequency measurements on both a 10 Gb/s Mach-Zehnder type modulator and a 40 Gb/s mode converter type modulator have been made. We have also derived the optical fields at the output of an electro-optic modulator when it is biased or operated in three different points in its transfer function. We showed that the sensitivity of our system is the highest when the DUT is operated at its minimum point. The electrical frequency responses measured using our system were in good agreement with $|S_{21}|$ measurements using vector network analyzers with calibrated wide band photodiodes. In addition, the harmonic rejection feature of the system was described. With proper selection of f_m and f_s , our system rejects higher order harmonics due to the non-linearities generated in the DUT. Our system's frequency response is primarily limited by two factors. One is the frequency response of the wide band photodiode used and the frequency to which it is calibrated. The second is the system's dynamic range. Nonetheless, an improved design should be capable of increasing the signal strength and reducing the residual power at the output of the frequency shifter, enhancing the system's dynamic range.

References

- [1] Kazuto Noguchi, Osamu Mitomi, and Hiroshi Miyazawa, "Millimeter-wave Ti:LiNbO₃ optical modulators," *J. of Lightwave Technology*, vol. 16, No. 4, pp. 615-619, 1998.
- [2] M. M. Howerton, R. P. Moeller, A. S. Greenblatt, and R. Krahenbuhl, "Fully packaged, broad-band LiNbO₃ modulator with low drive voltage," *IEEE Photon. Technol. Lett.*, vol. 12, pp. 792-794, Jul. 2000.
- [3] K. Noguchi, O. Mitomi, H. Miyazawa, and S. Seki, "A broadband Ti:LiNbO₃ optical modulator with a ridge structure," *Journal of Lightwave Tech.*, vol. 13, pp. 1164-1168, Jun. 1995.
- [4] W. K. Burns, M. M. Howerton, R. P. Moeller, A. S. Greenblatt, and R. W. McElhanon, "Broad-band reflection travelling-wave LiNbO₃ modulator," *IEEE Photon. Technol. Lett.*, vol. 10, pp. 805-806, Jun. 1998.
- [5] F. Rahmatian, N. A. F. Jaeger, R. James, and E. Berolo, "An ultrahigh-speed AlGaAs-GaAs polarization converter using slow-wave coplanar electrodes," *IEEE Photon. Technol. Lett.*, vol. 10, pp. 675-677, 1998.
- [6] R. Spickermann, S. R. Sakamoto, M. G. Peters, and N. Dagli, "GaAs/AlGaAs traveling wave electrooptic modulator with electrical bandwidth greater than 40 GHz," *Electron. Lett.*, vol. 32, pp. 1095-1096, Jun. 1996.
- [7] T. Ido, S. Tanaka, M. Suzuki, M. Koizumi, H. Sano, and H. Inoue, "Ultra high-speed multiple quantum well electroabsorption optical modulators with integrated waveguides," *J. Lightwave Tech.*, vol. 14, pp. 2026-2034, Sept. 1996

- [8] K. K. Loi, X. B. Mei, J. H. Hodiak, C. W. Tu, and W. S. C. Chang, "38 GHz bandwidth 1.3 μm MQW electroabsorption modulators for RF photonic links," *Electron. Lett.*, vol. 34, pp. 1018-1019, May 1998.
- [9] D. Chen, H. Fetterman, A. Chen, W. H. Steier, L. R. Dalton, W. Wang, and Y. Shi, "Demonstration of 110 GHz electrooptic polymer modulators," *Appl. Phys. Lett.*, vol. 70, no. 25, pp. 3335-3337, 1997.
- [10] D. Chen, D. Bhattacharya, A. Udupa, B. Tsap, H. R. Fetterman, A. Chen, S. Lee, J. Chen, W. H. Steier, and L. Dalton, "High-frequency polymer modulators with integrated finline transitions and low V_{π} ," *IEEE Phot. Tech. Lett.*, vol. 11, Jan. 1999.
- [11] W. Wang, D. Chen, H. R. Fetterman, Y. Shi, W. H. Steier, and L. R. Dalton, "60 GHz polymer electro-optic phase modulators," in Proc. 1995 Dig. LEOS Summer Topical Meet., RF Optoelectronics, WC2, pp. 5-6, Aug. 1995.
- [12] Tun S. Tan, Roger L. Jungerman, and Scott S. Elliott, "Optical receiver and modulator frequency response measurement with a Nd:YAG ring laser heterodyne technique," *IEEE Tran. On Microwave Theory and Techniques*, vol. 37, No. 8, pp. 1217-1222, 1989.
- [13] R. Thomas Hawkins II, Michael D. Jones, Steven H. Pepper, and Jeffery H. Goll, "Comparison of fast photodetector response measurements by optical heterodyne and pulse response techniques," *J. of Lightwave Technology*, vol. 9, No. 10, pp. 1289-1294, 1991.
- [14] P. D. Hale, T. S. Clement, and D. F. Williams, "Frequency response metrology for high-speed optical receivers," NIST, OFC, Mar. 2001.

- [15] Osamu Mitomi, Kazuto Noguchi, and Hiroshi Miyazawa, "Estimation of frequency response for high-speed LiNbO_3 optical modulators," *IEE Proc. -Optoelectron.*, vol. 146, No. 2, pp. 99-104, April 1999.
- [16] Frank Bowman, "*Introduction to Bessel functions*," Dover, NY, 1958.
- [17] George B. Arfken, and Hans J. Weber, "*Mathematical methods for physicists*," Harcourt, San Diego, 2001.
- [18] C. J. Tranter, "*Bessel functions with some physical applications*," The English Universities Press LTD., London, 1968.

Chapter 3

Summary, Conclusions, and Recommendations for Future Work

3.1. Summary and Conclusions

A wide band, cost effective system for measuring the frequency responses of electro-optic intensity modulators in the millimeter-wave regime has been described. The theory on which the system is based has also been described, and measurements on two high-speed electro-optic intensity modulators, including a 10 Gb/s LiNbO₃ Mach-Zehnder type and a 40 Gb/s GaAs mode-converter type modulator, have been made up to 65 and 78 GHz, respectively. The optical field expressions at the output of the modulator when it was operated at three different points on its transfer function have been presented. It was shown that the highest sensitivity of the system could be obtained by operating, or biasing, the DUTs at their minimum points. In addition, the harmonic rejection feature of the system and the requirements for achieving the harmonic rejection have been described. The technique for measuring the frequency response of an electro-optic intensity modulator using a vector network analyzer has also been presented.

The cost effective aspect of this measurement system has been achieved by using the method of optical heterodyning. Instead of using a costly wide bandwidth microwave sweeper to drive the DUT at millimeter-wave frequencies, the method of generating a millimeter-wave by mixing two tunable lasers in a wide band photodiode has been used.

The frequency response of the system is limited by the frequency response of the wide band photodiode used in the optical heterodyning and the frequency to which it is calibrated. Moreover, a wide band microwave amplifier is not required to increase the power of the millimeter-wave signals generated in order to make the wide band measurements, which is a costly component. Finally, all of the EDFAs and three of the polarization controllers could be eliminated in an improved and dedicated system, as will be explained in section 3.2. Moreover, the need of an electrical spectrum analyzer could also be eliminated. Eliminating these components would further reduce the overall cost of the system.

The system has shown the ability to make wide band measurements on both a Mach-Zehnder and a mode converter modulator. The experimental results showed the frequency responses of a 10 Gb/s and a 40 Gb/s modulator up to 65 GHz and 78 GHz, respectively. These frequency ranges are wider than those measured using the VNAs. To further increase the frequency range of the system as the speed of the modulators continuous to increase, the system needs only to use a photodiode with a wider bandwidth. Photodiodes with bandwidth of 75 GHz are currently commercially available. Such photodiodes should allow measurements approaching, if not exceeding, 100 GHz. In addition, the frequency responses measured by the system have been in close agreement with the responses measured using the two VNAs. Furthermore, the system has a higher dynamic range than that of the VNAs, as is described in Appendix E.

In conclusion, the experiments indicate that the system can measure the frequency responses of electro-optic intensity modulators in the millimeter-wave regime. The system provides a wide band, cost effective method to measure accurately the frequency

responses of the modulators. It also has the potential to increase its frequency range by using wider band photodiodes.

3.2. Recommendations for Future Work

There are three main recommendations for improving the performance and for reducing the cost of the measurement system. They are, designing a better frequency shifter, using polarization maintaining (PM) 50/50 optical couplers, and eliminating the electrical spectrum analyzer.

The first recommendation is to design a better frequency shifter so that it can output optical fields with both higher power and higher signal-to-noise ratio (SNR). The increase in both power and SNR of the optical field at the output of the frequency shifter can strengthen the frequency response signal and, in turn, increase the frequency range of the system. Possible frequency or wavelength shifters can be found in the literature, see for example [1-2].

The second recommendation is to use three polarization maintaining optical couplers to replace the two single mode 50/50 optical couplers connected to the lasers and the one used for the optical heterodyning. This would eliminate the need for three of the polarization controllers used in the system and preserve more optical power for heterodyning. Moreover, the sensitivity of the system would be enhanced since more microwave power would be generated by the wide band photodiode.

The last recommendation is to develop an electrical signal measurement system to replace the electrical spectrum analyzer used in the system. A possible design is to down-convert the response signal at the shift frequency to an IF frequency signal using an RF mixer. An electrical amplifier is needed to boost up the power of the IF signal and the signal at the IF frequency can be easily measured using a voltmeter. The other

suggestion is to measure the response signal at the shifter frequency using a square law detector and a voltmeter.

Moreover, developing an automated GPIB/HPIB data acquisition system using LabView would reduce the time to collect the response data. Using a local oscillator that outputs a signal at the shift frequency to replace the RF source used in the system would further reduce the cost of the system.

For further research in this field, the development of a system to measure the phase response of the electro-optic intensity modulators is recommended [3]. Users would be able to fully measure an electro-optic intensity modulator's S_{21} if we could develop a phase response measurement system. It is believed that the design of this system would provide strategy or clues to the design of the phase response measurement system.

References

- [1] S. T. Winnall, A. C. Lindsay, and G. A. Knight, "A wide-band microwave photonic phase and frequency shifter," *IEEE Tran. On Microwave Theory and Techniques*, vol. 45, No. 6, pp. 1003-1006, Jun. 1997.
- [2] F. Agullo-Lopez, J. M. Cabrera, and F. Agullo-Rueda, Electrooptics Phenomena, Materials and Applications, Academic Press, Inc., London, Great Britain, 1994, pp.198
- [3] Private discussion with Dr. Nicolas A. F. Jaeger.

Appendices

Appendix A: Optical Heterodyning

An optical heterodyning system uses a pair of tunable lasers, a polarization controller, a 50/50 optical coupler and a wide band photodiode. Figure A.1 shows an optical heterodyning system. The polarization controller is used to adjust the orientation of the polarization angle in one fiber so that it aligns with the polarization angle in the other fiber.

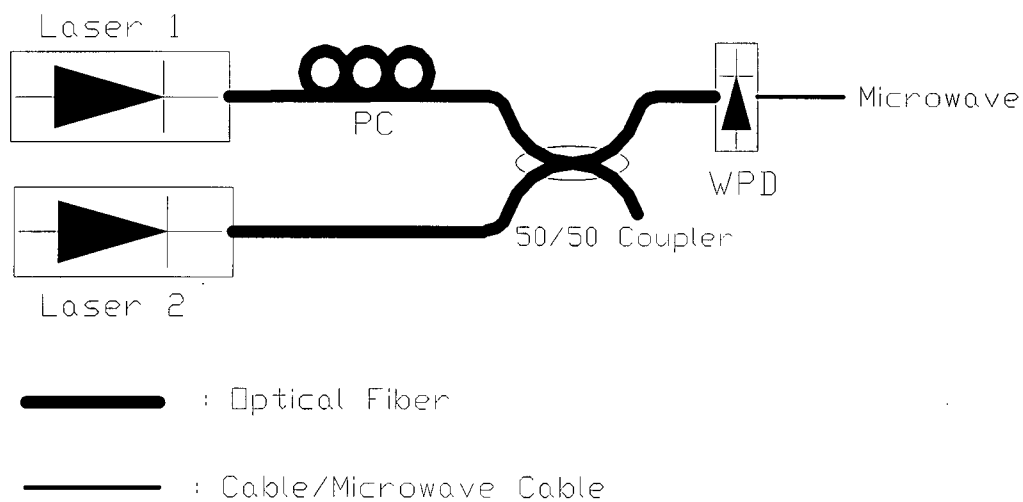


Figure A.1. A setup of an optical heterodyne system. PC: Polarization Controller, WPD: Wide band Photodiode.

The following mathematical description shows how a microwave or a millimeter-wave can be generated in the system shown in Figure A.1. The operating wavelengths and the corresponding frequencies of lasers 1 and 2 can be related by the following expressions,

$$f_1 = \frac{c}{\lambda_1}$$

and

$$f_2 = \frac{c}{\lambda_2}$$

where f_1 and f_2 are the optical frequencies, λ_1 and λ_2 are the operating wavelengths of lasers 1 and 2, respectively, and c is the speed of light. The optical fields at the output of lasers 1 and 2, E_1 and E_2 , can be expressed as

$$E_1(t) = A_1 e^{j2\pi f_1 t}$$

and

$$E_2(t) = A_2 e^{j2\pi f_2 t},$$

respectively, where A_1 and A_2 are the amplitudes of the lasers. At the output of the wide band photodiode, the photocurrent can be expressed as,

$$i = R_{DC} \rho (E_1 + E_2) \cdot (E_1^* + E_2^*).$$

Substituting the expressions of the optical fields, E_1 and E_2 , into the equation above, the photocurrent, i , at the output of the wide band photodiode can then be expressed as

$$i = R_{DC} \{A_1^2 + A_2^2 + 2\rho A_1 A_2 [\cos(2\pi f_m t) + \cos(2\pi f_s t)]\},$$

or

$$i = R_{DC} [P_1 + P_2 + 2 \cdot \rho \cdot \sqrt{P_1 P_2} \cdot \cos(2\pi f_m t)]$$

where $P_1 = A_1^2$ and $P_2 = A_2^2$ [1] are the optical powers that reach the wide band photodiode from lasers 1 and 2, R_{DC} and ρ are the DC responsivity and the calibrated frequency response of the wide band photodiode, respectively, f_m is the difference frequency, i.e., $f_m = f_1 - f_2$, or $f_m = f_2 - f_1$, and f_s is the sum of the two optical frequencies, i.e., $f_s = f_1 + f_2$. Since the frequency response of the wide band photodiode, ρ , approaches zero as the frequency is in the terahertz range, the term, $2\rho A_1 A_2 \cos(2\pi f_s t)$, is zero. In the system described in Chapter 2, the difference frequency, f_m , is achieved by keeping λ_2 constant (f_2 is constant) and increasing λ_1 (f_1 is decreased). Therefore, f_m , is expressed as

$$f_m = f_2 - f_1.$$

Appendix B: The Frequency Shifter

The frequency shifter used consists of a Mach-Zehnder modulator and an optical bandpass filter made up by cascading two Bragg grating filters. The shifter generates an optical signal to down-convert the higher frequency first sideband of the DUT to a constant microwave frequency, at which the response signal is measured. Moreover, it “rejects” higher order harmonics generated by the DUT. The frequency shifter used in the system was inexpensive to implement and readily available in our laboratory. Figure B.1 shows a diagram of the setup of the frequency shifter used in the measurement system.

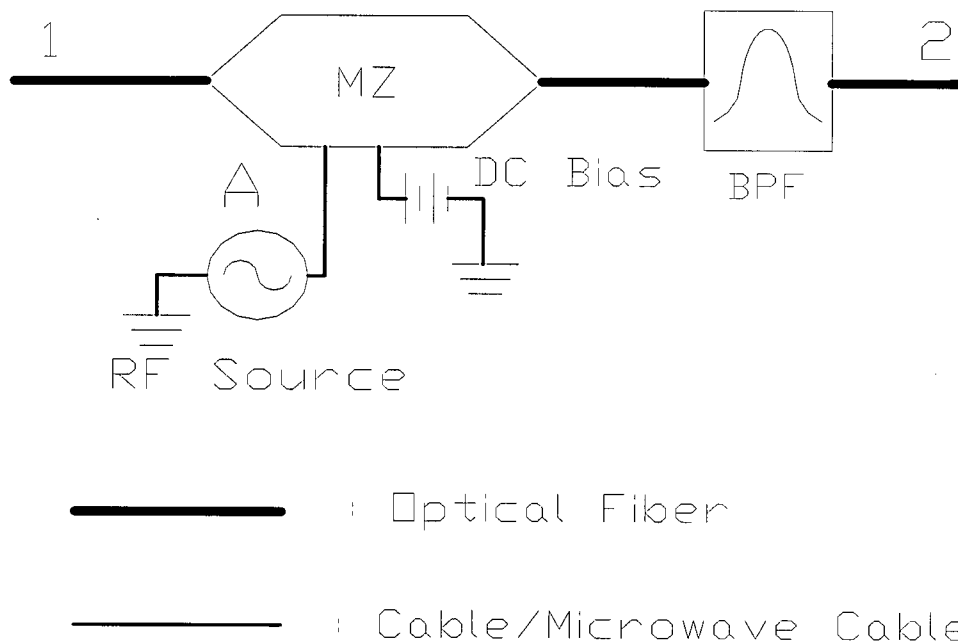


Figure B.1. Diagram showing the setup of the frequency shifter used in the measurement system. 1: optical frequency (f_2), 2: shifted optical frequency ($f_2 - f_s$), A: the shift frequency (f_s), MZ: Mach-Zehnder, BPF: Optical Bandpass filter.

The Mach-Zehnder used in the frequency shifter was a 10 Gb/s LiNbO₃ modulator. It was driven by a 18 dBm, 2.4 GHz signal. The modulator was operated, or biased, at its minimum point to maximize the amplitudes of the first sidebands and to suppress the carrier. The center wavelength of the cascaded Bragg grating filters was measured to be at ~1558.58 nm and the 3-dB pass-band of the filters was measured to be ~1558.47 nm to ~1558.66 nm, see Figure B.2.

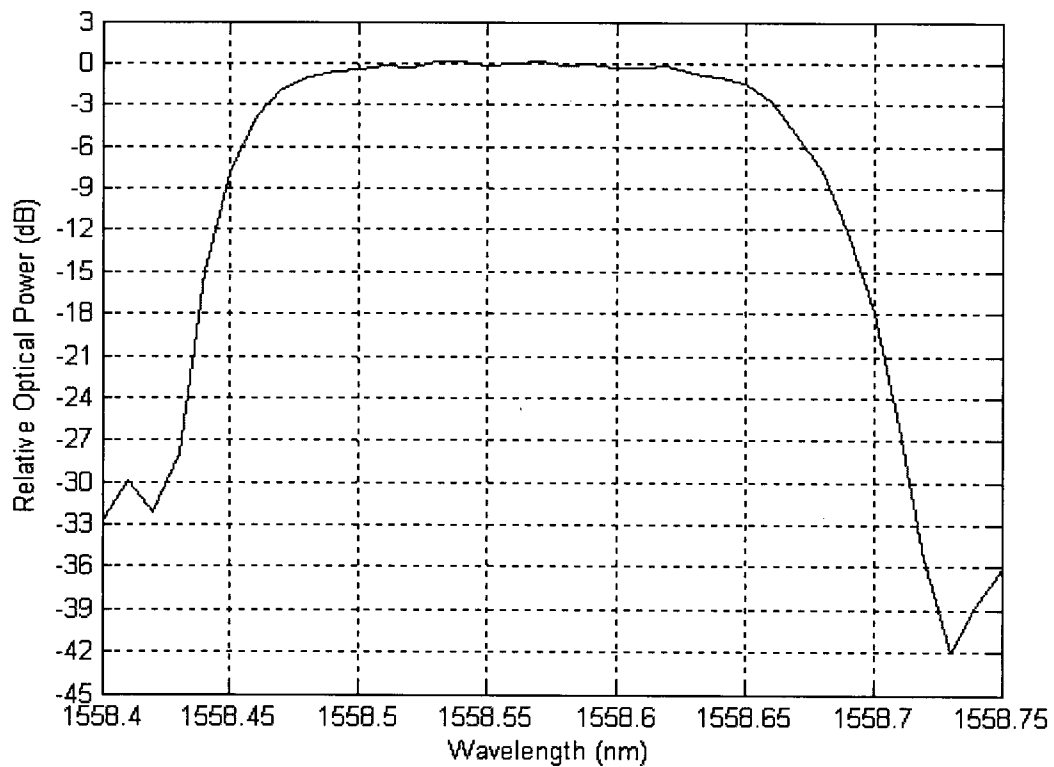


Figure B.2. The 3-dB pass-band of the filter was measured to be ~1558.47 nm to ~1558.66 nm.

The pass-band of the filter was used to determine the setting of the operating wavelength of the laser (laser 2) that supplied an optical source to the frequency shifter. The operating wavelength of laser 2 was set so that the lower frequency first sideband optical field of the Mach-Zehnder was passed while its carrier and its higher frequency first sideband were filtered out. The use of two cascaded Bragg gratings provided better filtering of the carrier so that the power due to the mixing of the residual carrier and the lower frequency first sideband was minimized at the shift frequency, f_s . Nevertheless, the lower frequency first sideband, the residual carrier and the other higher order sidebands that were passed mixed with the optical fields at the output of the DUT. One can easily select f_s and f_m to ensure that none of higher order harmonics that are due to the mixing of these sidebands with the optical field at the output of the DUT is shifted to f_s , as will be explained in Appendix C below.

Figure B.3 shows the spectrum of the optical components from the frequency shifter and the DUT (the 10 Gb/s modulator) for a difference frequency of ~ 30 GHz. Figure B.4 shows the system that is used to obtain the optical fields shown in Figure B.3.

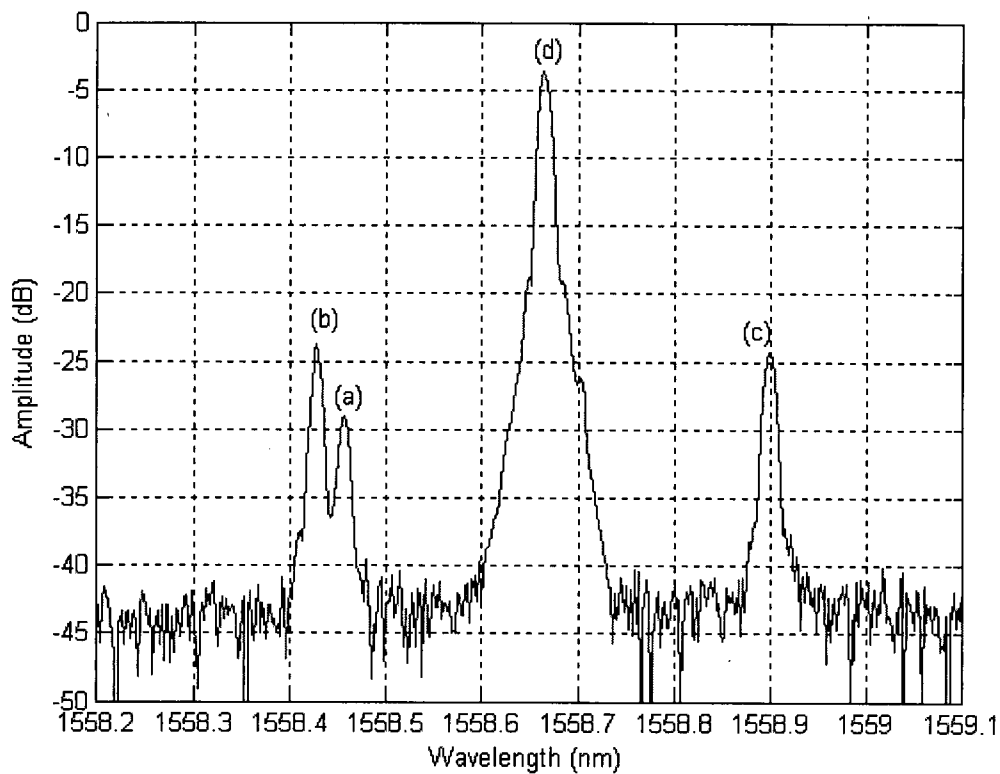


Figure B.3. Spectrum of the optical components from the frequency shifter and the DUT. a) The component from the frequency shifter, b) the high frequency sideband from the DUT, c) the low frequency sideband from the DUT, d) the optical carrier from the DUT. (Setting of the ANDO AQ6317B optical spectrum analyzer: RBW = 0.01 nm, Span = 1 nm)

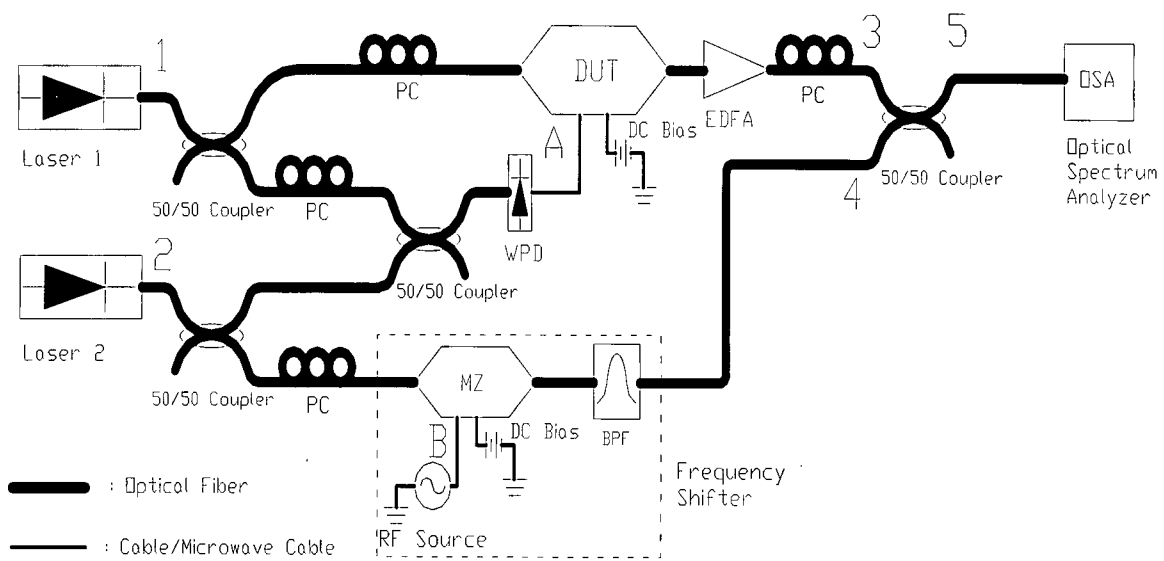


Figure B.4. Diagram showing the system used to obtain the optical field shown in Figure B.3.

The optical spectrum shown in Figure B.4 was obtained using an ANDO AQ6317B optical spectrum analyzer. The wavelength of laser 2 was set at ~1558.42 nm. As can be seen, the optical field at the output of the frequency shifter can be found at ~1558.45 nm, that is approximately equal to the wavelength of the lower frequency first sideband of the frequency shifter, i.e., the sum of 1558.42 nm and the shift frequency (2.4 GHz \cong 0.02 nm). The wavelength offset of about 0.01 nm is due to the offset of the laser and the optical spectrum analyzer. The optical carrier and the two first sidebands of the DUT can be found at ~1558.66 nm, and ~1558.90 nm and ~1558.42 nm. The difference frequency can be confirmed using this equation,

$$f_m \cong \frac{1.25}{0.01} \cdot |\lambda_1 - \lambda_s|$$

where λ_1 is the wavelength of the optical carrier of the DUT (or the operating wavelength of laser 1), and λ_s is the wavelength of one of its first sidebands. The coefficient, 1.25/0.01, denotes the conversion ratio of the electrical frequency in gigahertz to the wavelength in nanometer for $\lambda_1 \approx 1550$ nm.

Appendix C: Harmonic Rejection Requirements

As stated in Chapter 2, the measurement system can “reject” higher order harmonics, due to the non-linearities, generated in the DUT. This appendix describes how the higher order harmonics are rejected and lists the requirements for achieving the rejection property.

When the DUT is driven by an RF, or microwave, signal with the difference frequency, f_m , and the optical input to the DUT is supplied by a light source with the optical frequency, f_1 , the optical frequencies of the sidebands and the carrier at the output of the DUT are $f_1 + 4f_m$, $f_1 + 3f_m$, $f_1 + 2f_m$, $f_1 + f_m$, f_1 , $f_1 - f_m$, $f_1 - 2f_m$, $f_1 - 3f_m$, $f_1 - 4f_m$, or $f_1 \pm nf_m$, where $n = 0, \pm 1, \pm 2, \pm 3, \pm 4$ (see equation (20) in Chapter 2). At the output of the frequency shifter, the lower frequency first sideband at optical frequency, $f_2 - f_s$, and other sidebands at $f_2 - kf_s$, where k is any positive integers, are produced. Table C.1 shows the frequencies of the electrical signals at the output of the low frequency photodiode generated due to the mixing of the optical fields at the output of the frequency shifter with the optical fields at the output of the DUT. Note that the optical fields at $f_2 - kf_s$ are negligibly small and are not shown for $k > 4$. The optical fields with frequencies greater than $f_1 + 2f_m$ and optical fields with frequencies less than $f_1 - 2f_m$ at the output of the DUT are not shown since they are also negligibly small.

Frequencies of the signal at the output of the DUT					
Frequencies of the signal at the output of the frequency shifter	$f_1 + 2f_m$	$f_1 + f_m$	f_1	$f_1 - f_m$	$f_1 - 2f_m$
f_2	$-f_m$	DC	f_m	$2f_m$	$3f_m$
$f_2 - f_s$	$-f_m - f_s$	f_s	$f_m - f_s$	$2f_m - f_s$	$3f_m - f_s$
$f_2 - 2f_s$	$-f_m - 2f_s$	$2f_s$	$f_m - 2f_s$	$2f_m - 2f_s$	$2f_m - 2f_s$
$f_2 - 3f_s$	$-f_m - 3f_s$	$3f_s$	$f_m - 3f_s$	$2f_m - 3f_s$	$2f_m - 3f_s$
$f_2 - 4f_s$	$-f_m - 4f_s$	$4f_s$	$f_m - 4f_s$	$2f_m - 4f_s$	$2f_m - 4f_s$

Table C.1. Table showing the frequencies of the electrical signals at the output of the low frequency photodiode generated due to the mixing of the optical fields at the output of the frequency shifter with the optical fields at the output of the DUT.

According to Table C.1, all of the electrical signals in the second column will not be at f_s if $f_s \neq f_m$. The frequencies of electrical signals in the third column will not be at the shift frequency, except the one that measures the frequency response of the DUT. In the fourth column, the frequencies of the electrical signals generated can be expressed as $f_m - kf_s$, where k is any positive integers greater than or equal to zero. Here, the electrical signals will not be at the shift frequency, f_s , if $f_s \neq \frac{1}{k}f_m$. Therefore, to reject these signals, one must select $f_s \neq \frac{1}{k}f_m$. Similarly, one must select $f_s \neq \frac{2}{k}f_m$ for the fifth column. For the last column, one must select $f_s \neq \frac{3}{k}f_m$ to reject the higher order harmonics. Therefore, in general, one must select $f_s \neq \frac{q}{r}f_m$, where q and r are any integers greater than zero, to ensure that none of the higher order harmonics is shifted to f_s .

Appendix D: Electro-optic Intensity Modulator Frequency Response Measurement using Vector Network Analyzer

A VNA can measure the magnitude and phase characteristics of networks and of components such as filters, attenuators and antennas. Also, it is commonly used to measure S_{21} of an electro-optic intensity modulator. To do that, the VNA is first calibrated to remove unwanted effects of the cables and other components in the measurement path. Once the calibration is performed, a measurement setup, shown in Figure D.1, is used to measure the frequency response of a DUT.

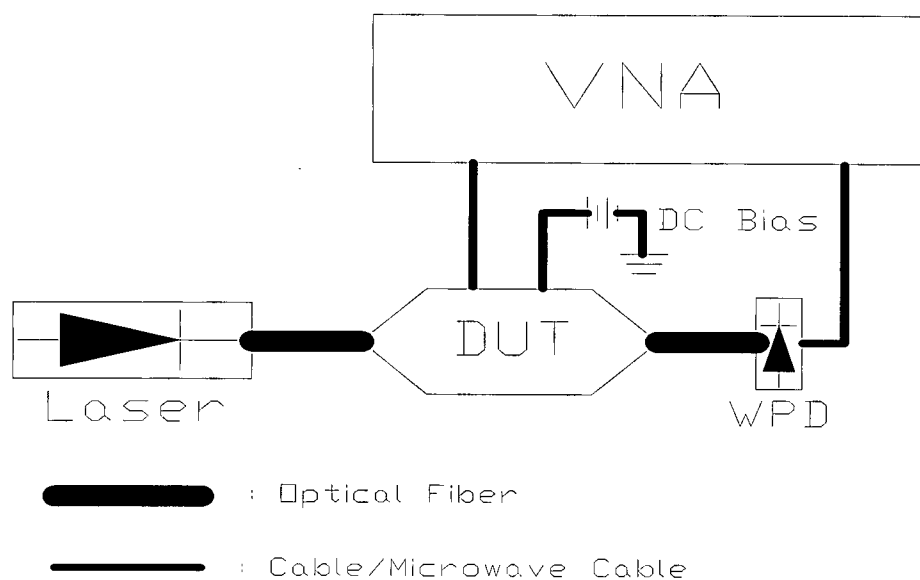


Figure D.1. The measurement setup used to measure the frequency responses of the DUTs in chapter 2. WPD: Wide Band Photodiode.

The following shows a mathematical description of how the frequency response of a DUT is measured using a VNA. Here we assume a balanced electro-optic intensity modulator with the following transfer function, i.e., with zero intrinsic bias [2]

$$I_{out}(V) = I_o \cos^2\left(\frac{\pi V}{2V_\pi}\right) \quad (1)$$

where I_o is the maximum output intensity, V_π is the half-wave voltage of the modulator, and V is the applied voltage given by

$$V = V_{DC} + V_{RF} \equiv V_{DC} + V_m \cos(2\pi f_m t) \quad (2)$$

where V_{DC} is a DC voltage, V_{RF} is an RF voltage, V_m and f_m are the amplitude and the frequency of the RF, or microwave, signal.

Substituting equation (2) into (1), the optical field at the output of the modulator can be expressed as

$$E_{out} = 2\sqrt{\frac{\mu_o}{\varepsilon}} I_{out}^{1/2}(V) = 2\sqrt{\frac{\mu_o}{\varepsilon}} I_o^{1/2} \cos(\phi_{DC} + \phi_{RF}) \cdot e^{j2\pi f t} \quad (3)$$

where μ_o is the permeability of free space, ε is the permittivity of the material,

$$\phi_{DC} = \frac{\pi V_{DC}}{2V_\pi} \text{ and } \phi_{RF} = \frac{\pi V_m}{2V_\pi} \cos(2\pi f_m t), \text{ or } \phi_{RF} = M \cos(2\pi f_m t), \text{ i.e., } M = \frac{\pi V_m}{2V_\pi}, \text{ and } f$$

is the frequency of the light. The term $\cos(\phi_{DC} + \phi_{RF})$ can be expressed using Taylor expansion and Bessel functions about the microwave frequency, f_m , see for example [3-5],

$$\begin{aligned} \cos(\phi_{DC} + \phi_{RF}) = & \cos \phi_{DC} \left\{ J_0(M) + 2 \sum_{n=1}^{+\infty} (-1)^n J_{2n}(M) \cos[2n(2\pi f_m t)] \right\} \\ & - \sin \phi_{DC} \left\{ -2 \sum_{n=1}^{+\infty} (-1)^n J_{2n-1}(M) \cos[(2n-1)(2\pi f_m t)] \right\} \quad (4) \end{aligned}$$

where J_n is the Bessel function of the first kind of order n .

From equations (3) and (4), the optical field at the output of the modulator can be expressed as

$$\begin{aligned} E_{DUT} = & 2 \sqrt{\frac{\mu_o}{\epsilon}} I_o^{1/2} \left\{ \cos \phi_o [J_0(M) - 2J_2(M) \cos(4\pi f_m t) + 2J_4(M) \cos(8\pi f_m t) - \dots] \right. \\ & \left. - \sin \phi_o [2J_1(M) \cos(2\pi f_m t) - 2J_3(M) \cos(6\pi f_m t) + 2J_5(M) \cos(10\pi f_m t) - \dots] \right\} \cdot e^{j2\pi f t} \quad (5) \end{aligned}$$

The photocurrent at the output of the wide band photodiode, due to the optical field in equation (5), is

$$i_{pd} = R_{pd} \rho_{pd} (E_{DUT} \cdot E_{DUT}^*) \quad (6)$$

and the voltage is

$$V \propto \frac{i_{pd}}{R_{pd} \rho_{pd}} = 4 \frac{\mu_o}{\varepsilon} I_o (V_{DC} + V_{if_m} + V_{jf_m} + V_{kf_m}) \quad (7)$$

where

$$V_{if_m} = \sin(2\phi_{DC}) [J_0(M)J_i(M) + J_1(M)J_{i+1}(M) + J_2(M)J_{i+2}(M) + J_3(M)J_{i+3}(M) + \dots] \cdot \cos(2\pi if_m t) \quad (8)$$

$$V_{jf_m} = [\sin \phi_{DC} J_{j/2}^2(M) + 2 \cos \phi_{DC} \cdot J_0(M)J_j(M) + 2 \sin \phi_{DC} J_1(M)J_{j+1}(M) + 2 \cos \phi_{DC} J_2(M)J_{j+2}(M) + 2 \sin \phi_{DC} J_3(M)J_{j+3}(M) + \dots] \cdot \cos(2\pi jf_m t) \quad (9)$$

$$V_{kf_m} = [\cos \phi_{DC} J_{k/2}^2(M) + 2 \cos \phi_{DC} J_0(M)J_k(M) + 2 \sin \phi_{DC} J_1(M)J_{k+1}(M) + 2 \cos \phi_{DC} J_2(M)J_{k+2}(M) + 2 \sin \phi_{DC} J_3(M)J_{k+3}(M) + \dots] \cdot \cos(2\pi kf_m t), \quad (10)$$

and the subscripts, DC , if_m , jf_m , and kf_m are the frequencies of the voltages, $i = 1, 3,$

$5, 7, \dots, j = 2, 6, 10, 14, \dots$, and $k = 4, 8, 12, 16, \dots$. The VNA measures $4 \frac{\mu_o}{\varepsilon} I_o V_{f_m}$ (i

$= 1$) at its receiving port and the voltage to the DUT, V_m , at its output port. The

relationship, $20 \cdot \log \frac{V_{f_m}}{V_{in}}$, gives $|S_{21}|$ in dBe. To obtain the highest signal strength, the

DUT is best operated at its quadrature point (i.e., $\phi_{DC} = \pi/4$) on its transfer function such

that the term, $\sin(2\phi_{DC})$, is maximized in equation (8).

Appendix E: Comparison of the System Dynamic Range of our System to that of a VNA

Here we compare the system dynamic range (SDR) of our measurement system and that of the 50 GHz Agilent 8510C VNA (microwave section: 85107B) that was used to measure the $|S_{21}|$ of the 10 Gb/s modulator in Chapter 2. (Note that both our system and the VNA used the wide band photodiode manufactured by Discovery Semiconductor Inc.) The SDR is the amount of attenuation that can be measured from a 0 dB reference [6]. For the VNA and our system, it is the difference of the power at the output point, P_{ref} , and the minimum power that can be measured above the noise floor at the receiving point, P_{min} , i.e., $SDR = P_{ref} - P_{min}$ in dB [6]. For the 50 GHz VNA, P_{ref} is the power measured at the output port and P_{min} is the noise floor of the VNA; for our system, P_{ref} and P_{min} are the power generated in optical heterodyning and the residual signal power, respectively.

The SDR of our system is ~82 to ~79 dB for modulation frequencies below 55 GHz (this is the 3-dB frequency of the wide band photodiode and the maximum frequency for which the wide band photodiode was calibrated). On the other hand, the SDR of the 50 GHz VNA is between 60 dB and 89 dB depending on the modulation frequency [6]. Figure E.1 shows the SDR of our system as the asterisks and that of the VNA as the solid curve. As can be seen, the SDR of our system decreases by only 3 dB over the frequency range and is higher than that of the VNA for frequencies above ~20 GHz. The SDR of the VNA decreases by 29 dB over its 50 GHz span, and the decrease is due to the decrease of P_{ref} . This decrease in P_{ref} , and thus is the SDR, degrades the

VNA's performance over the frequency. The SDR of the Agilent new 110 GHz model N5250A performance network analyzer (PNA) is also shown as the dashdotted curve in Figure E.1, which has a high SDR over the 110 GHz span. Our system could have the similar SDR as that of the 110 GHz PNA if a wider band photodiode was used for the optical heterodyning.

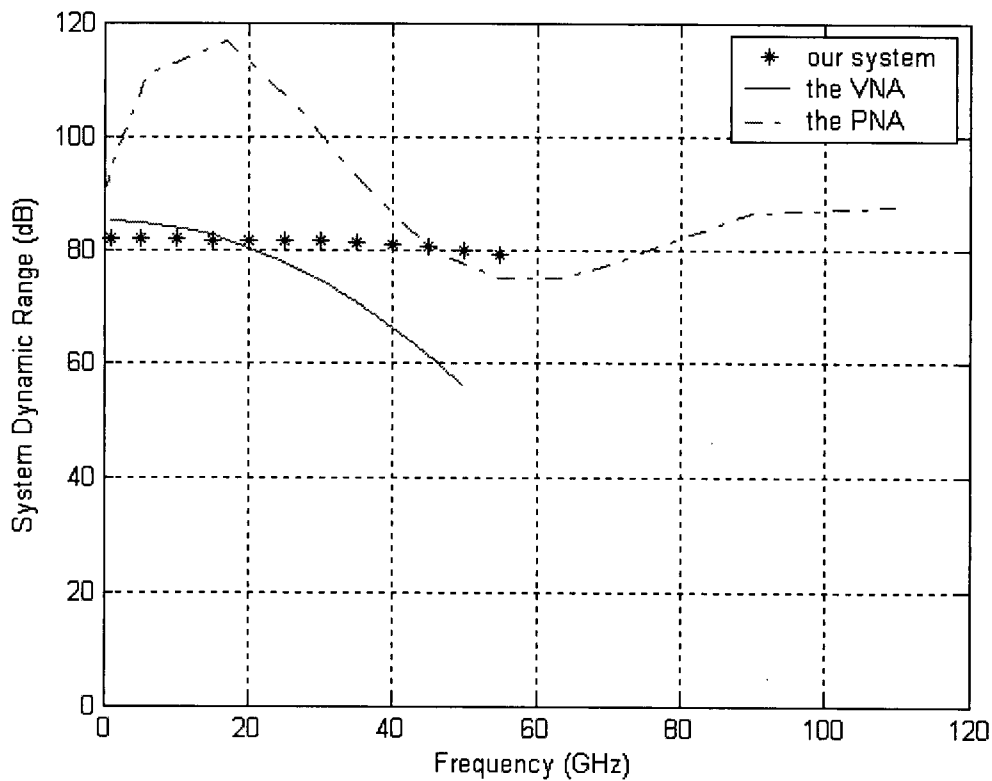


Figure E.1 Our system showing a higher system dynamic range than that of the 50 GHz VNA. The system dynamic range of the 110 GHz PNA is also shown.

Figure E.2 shows how the decrease of P_{ref} , and thus the SDR, affects the frequency range of the measurement using the 50 GHz VNA. When the laser shown in Figure D.1, in Appendix D, is turned off, the measured $|S_{21}|$ is shown as the dotted curve in Figure E.2. Since P_{ref} decreases by 29 dB, while the power at the receiving port is nearly constant (this power is due to the dark current at the output of the wide band photodiode), the measured $|S_{21}|$ for which the laser is off increases as shown in the figure. The dotted curve increases as frequency increases and it meets the frequency response of the DUT shown as the solid curve at ~ 45 GHz. Therefore, the measured, uncorrected frequency response of the DUT beyond ~ 45 GHz is overshadowed by the dotted curve. In contrast, the frequency response of the DUT measured using our system shows continual roll-off beyond 50 GHz as a result of the virtually constant power output from the wide band photodiode.

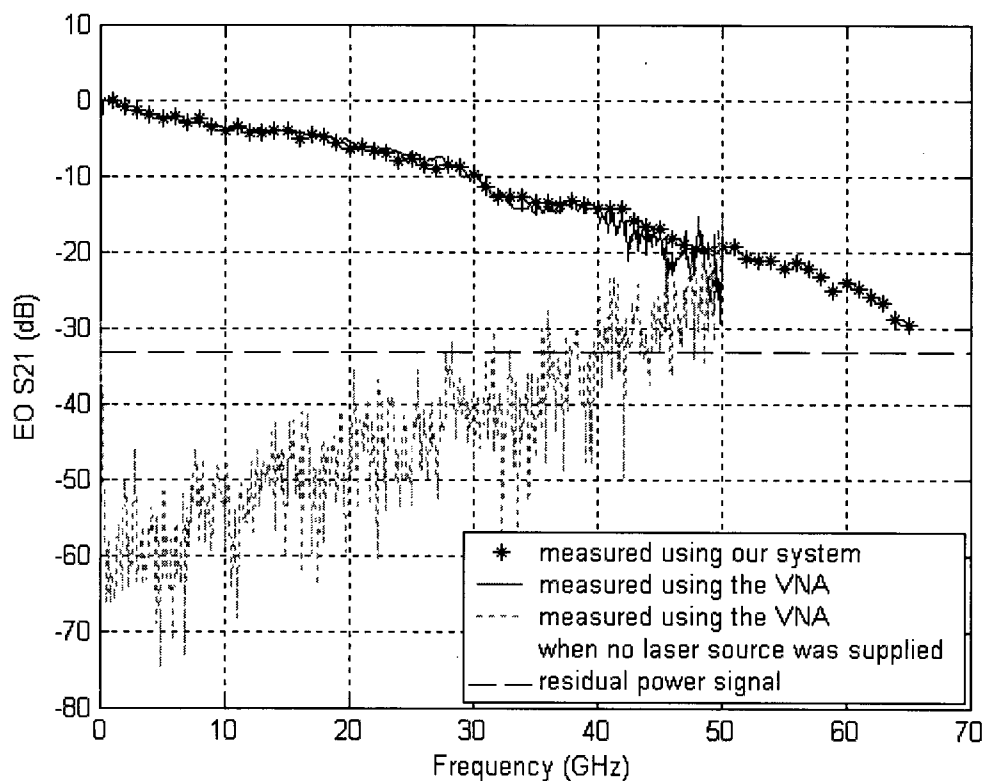


Figure E.2. The frequency response of the modulator when no laser source was supplied is shown as the dotted curve. It overshadowed the uncorrected frequency response of the 10 Gb/s modulator measured using the VNA, shown as the solid curve, starting at ~45 GHz. The uncorrected frequency responses of the 10 Gb/s modulator measured using our system, shown as the asterisks, shows continual roll-off beyond 50 GHz due to the virtually constant power output from the optical heterodyning and the constant residual power signal shown as the dashed line.

References

- [1] G. L. Li, and P. K. L. Yu, "Optical intensity modulators for digital and analog applications," *J. of Lightwave Technology*, vol. 21, No. 9, pp. 2010-2030, Sep. 2003.
- [2] Osamu Mitomi, Kazuto Noguchi, and Hiroshi Miyazawa, "Estimation of frequency response for high-speed $LiNbO_3$ optical modulators," *IEE Proc. -Optoelectron.*, vol. 146, No. 2, pp. 99-104, April 1999.
- [3] Frank Bowman, "*Introduction to Bessel functions*," Dover, NY, 1958.
- [4] George B. Arfken, and Hans J. Weber, "*Mathematical methods for physicists*," Harcourt, San Diego, 2001.
- [5] C. J. Tranter, "*Bessel functions with some physical applications*," The English Universities Press LTD., London, 1968.
- [6] "Agilent 8510C network analyzer," Data Sheet, Agilent Technologies, Palo Alto, CA.